

Efficient Conservation of the Brazilian Amazon: Estimates from a Dynamic Model*

Rafael Araujo[†] Francisco Costa[‡] Marcelo Sant'Anna[§]

December 10, 2024

Abstract

This paper estimates the Brazilian Amazon's carbon-efficient forest cover – i.e. when farmers internalize the social cost of carbon. We propose a dynamic discrete choice land-use model and estimate it using a panel of land use and carbon stock of 5.7 billion pixels between 2008 and 2017. The business-as-usual scenario implies an inefficient release of 42 billion tons of CO_2 in the long run resulting from the deforestation of an area twice the size of France. A carbon tax that makes farmers internalize the social cost of carbon would implement the efficient allocation and generate welfare gains exceeding 1.6 trillion dollars. Responses from a carbon tax are highly convex: a carbon tax of only \$10/ton would preserve 95% of the efficient carbon stock. An excise tax on cattle ranching, a second-best policy, achieves at most 87% of the first-best welfare gains.

JEL: Q23, Q54, Q15, C35, L73

Keywords: Deforestation, Carbon Emission, Amazon, Dynamic Discrete Choice Model.

*We thank Mike Abito, Juliano Assunção, Arthur van Benthem, Teevrat Garg, Torfinn Harding, Robert Heilmayr, Roozbeh Hosseini, Kelsey Jack, Felipe Jordan, Michael Kiley, Jose A. Scheinkman, Wolfram Schlenker, Paul Scott, Joseph Shapiro, Eduardo Souza-Rodrigues, and seminar participants at the NBER EEE Spring Meeting, ASSA-AEA Meeting, AERE Summer Conference, GoSee, Ridge EEE, Barcelona GSE Summer Forum, KDI Frontiers in Development, LSE Environment Week, Cowles Foundation Models and Measurement, Toulouse Conference on Economics of Energy and Climate, UCSB Occasional Workshop, joint MIT-Columbia-Stanford-Cornell Energy & Environmental Economics seminar, Wharton, University of Georgia, Insper, and FGV EPGE. We also thank Bård Harstad for excellent editorial advice and three anonymous referees. Financial support is gratefully acknowledged from Rede de Pesquisa Aplicada FGV and from Coordenação de Aperfeiçoamento de Pessoal de Nível Superior - Brasil (CAPES) - Grant #001.

[†]Sao Paulo School of Economics FGV EESP. E-mail: rafael.araujo@fgv.br.

[‡]FGV EPGE. E-mail: francisco.costa@fgv.br.

[§]FGV EPGE. E-mail: marcelo.santanna@fgv.br.

1 Introduction

Limiting global warming hinges on drastically reducing greenhouse gas emissions over the next decades. All but one of the mitigation pathways proposed in the last assessment of the Intergovernmental Panel on Climate Change rely on agriculture and land use reaching net-zero emissions by 2030 (Rogelj et al., 2018).¹ Reducing deforestation in tropical ecosystems is key to this endeavor because tropical forests hold an extraordinary amount of carbon. Deforestation releases this carbon into the atmosphere, which makes forest clearing the main source of CO_2 emissions in tropical regions. For instance, the Brazilian Amazon alone stored more than 200 billion tons of CO_2 in 2000. Since then, deforestation in the region has released over 17 billion tons of CO_2 (De Azevedo et al., 2018), the equivalent to 3.5 times the United States' total fossil fuel emissions in 2020.

While preserving tropical forests has great global social value, expanding the agricultural frontier may benefit the local population and contribute to regional development. The main driver of forest loss in the Brazilian Amazon has been the expansion of pasture for extensive cattle ranching. In our study period, between 2008 and 2017, 90% of the deforested area was converted to pasture for extensive cattle ranching, while most of the remaining deforested areas were converted to grow high-productivity cash crops, such as soy and maize. This indicates sizable spatial heterogeneity in the disposition of the private benefits from exploiting the land. Likewise, carbon is unevenly spread over the forest, representing a large spatial dispersion in the social cost of deforestation. These spatial heterogeneities imply that the trade-off between conservation and agriculture is essentially local and that policies blind to these spatial heterogeneities will lead to inefficient allocations.

In this paper, we estimate the carbon-efficient forest cover in the Brazilian Amazon. We then assess the effectiveness of environmental policies aimed at reducing emissions from land use change and compare the welfare implications of first-best policies, which are based on the carbon content of the forest, and second-best policies. To do so, we propose a dynamic discrete choice model where profit-maximizing farmers choose the land use considering location-specific factors, such as conversion costs, flow returns, and the option value of future land use. In our model, the carbon-efficient land use is the one in which farmers fully internalize the social value of the carbon stored in the forest when choosing whether to preserve the vegetation or convert it into pasture or cropland. We restrict attention to this precise definition of efficiency because we use high-resolution spatial measurements of aboveground biomass stored in each plot of the forest.

¹The only exception is the scenario in which carbon dioxide removal technologies are available at a massive scale by 2050 (mitigation pathway S5 in Rogelj et al., 2018).

Our model generates land use transition probabilities which depend on observed and unobserved state variables and primitive parameters. We recover primitive parameters by using the flow of observed land-use choices, following steps similar to Scott (2013). Specifically, we derive an Euler equation that serves as a regression in which land-use transition probabilities form the dependent variable. Furthermore, the panel structure of the data allows us to account for fixed local unobservables during estimation. This model-based regression is the cornerstone of our estimation to recover the model’s structural parameters.

We estimate the model using a panel dataset that classifies the land use of more than 5.7 billion pixels – at 30 meters resolution – for each year from 2008 to 2017 in the Brazilian Amazon (MapBiomass, 2019). We model the return of agriculture by combining potential yield for each crop (FAO GAEZ, 2012) with price data of agricultural products at major regional trade hubs, and newly computed transportation costs.² The amount of aboveground biomass stored in the vegetation of each 30-meter pixel (Zarin et al., 2016) is the key location-specific variable that allows us to estimate the efficient forest cover and to study carbon-based policies. We focus on forested pixels outside protected areas because protected areas are subject to specific regulations.

We compute the carbon-efficient steady-state forest cover as the one in which agents fully internalize the social cost of carbon of \$50 per ton of CO_2 (EPA, 2016). Our counterfactuals show a gap in steady-state emissions under the business-as-usual (BAU) and the efficient land use of 42 billion tons of CO_2 . This implies the Brazilian Amazon under BAU land use would *inefficiently* release nine times the annual fossil fuel emissions of the United States. In the long run, the Brazilian Amazon would be short 1,186,000 km^2 of forest cover to its efficient steady state – an area approximately twice the size of France. We calculate the welfare loss between the BAU and efficient land use paths at approximately 1.66 trillion dollars, mostly driven by over 2 trillion dollars in social damages from inefficient emissions.

Our framework also allows us to evaluate the evolution of land use under the efficient and BAU long-run transitions, considering the role of forest regeneration. We find forest regeneration has little impact on the efficient path. This implies that the efficient carbon stock is mainly achieved by conserving native forests, especially those with high carbon density. However, regeneration plays a substantial role in the BAU land use path, reflecting current practices that lead to field exhaustion and abandonment. Neglecting regeneration increases the efficient emission gap by 42% after 15 years of BAU land use.

We investigate two policy instruments to set land use closer to its carbon-efficient path.

²We estimate transportation costs for each crop from each pixel to international markets following Donaldson (2018). We build a complete transportation network in Brazil including roads, ports, and waterways. We then fit a non-linear least squares model of freight cost to monetize transportation costs.

We calculate how a tax based on the potential carbon stock of a given location could shape farmers' incentives to deforest. This policy can be interpreted as an implied carbon tax (or subsidy) that changes the private forest return – e.g., increased enforcement or providing payment for ecosystem services based on the carbon preserved in the forest. This carbon tax is the first-best policy instrument and would implement the carbon-efficient steady-state land use if it equates the private carbon return to the social cost of carbon. We find a convex land-use response from a carbon tax – relatively small increases in the perceived value of carbon substantially mitigate emissions. For example, a carbon tax of \$2.5 per ton of CO_2 stored in the forest would prevent 25 billion tons of CO_2 from being released in the steady state, implementing 60% of the socially efficient carbon emission reduction relative to BAU land use. A carbon tax of \$5 per ton would preserve 34 billion tons of CO_2 , mitigating 81% of the inefficient emissions in the steady state. Intuitively, land is the main input for the expansion of cattle ranching, so relatively small increases in the perceived cost of deforesting the marginal plot represent a substantial increase in the cost structure of ranchers.

Alternatively, we consider excise taxes on cattle ranching and crops. These are second-best policy instruments for carbon mitigation as they do not directly tie to the forest's carbon density. Our counterfactuals show that a 20% tax on cattle ranching returns would mitigate 15 billion tons of CO_2 in emissions. Our welfare calculations indicate that a 100% tax on cattle returns is the second-best policy, and it achieves 87% of the first-best welfare gains. This is predominantly driven by the second-best policy implementing substantial emission reductions (worth 1.8 trillion dollars in damages). Taxing crops has virtually no effect on emissions, as crops account for a small share of the region's land use.

It is worth emphasizing that our analysis pertains exclusively to the social costs imposed by the aboveground forest carbon stock. However, forest conservation has additional social benefits as forests hold immeasurable biodiversity value, regulate regional precipitation (Spracklen et al., 2012; Staal et al., 2018), preserve biomass in peatlands, and avoid ecosystems reaching tipping points (Nobre et al., 1991; Flores et al., 2024). Considering these other factors, we should read our estimates as lower bounds for the efficient gap. This limitation stems from available data concerning these other externalities and not from our approach, which can easily accommodate them once more reliable measurements become available.

This paper belongs to the emerging literature using discrete choice models to study forest conservation policies (e.g., Heilmayr et al., 2020; Dominguez-Iino, 2021; Hsiao, 2021; Araujo, 2022). Most of these papers employ static models of land use estimated with cross-sectional data. This is the case of Souza-Rodrigues (2019), which studies the demand for deforestation in private properties in the Brazilian Amazon. As in our paper, the author uses the model to investigate permanent policy changes and their long-run implications for the forest. Using

2006 census data, Souza-Rodrigues (2019) finds that policies that are blind to the spatial heterogeneity of the carbon stored in the forest, such as payments for preserved areas and land taxes, can effectively reduce deforestation.

Our main contribution is to introduce a dynamic and spatially detailed framework to study carbon conservation in the Amazon rainforest. By recognizing the inherently local nature of forest conservation – and accounting for spatial heterogeneity in both land returns and carbon storage –, we disentangle the loss of forest cover from CO_2 emissions to assess the cost-effectiveness of policies directly linked to the potential carbon content of the land. This allows us to investigate the potential of carbon tax within a policy debate dominated by quantity restrictions and direct regulation.³ Our approach based on a dynamic model further allows us to decompose the effects of conservation and forest regeneration. We find that the efficient land-use path is primarily driven by conservation, but regeneration plays an important role in the BAU path. Our welfare analysis decomposes the social gains and private losses under first- and second-best policy instruments, shedding light on the distributional consequences of various policy options. Last, our analysis confirms that models based on static approaches underestimate land use elasticities (Scott, 2013). This means preserving carbon in the long run may be cheaper than previously thought.⁴

A related literature studies land-use decisions using static general equilibrium environments (*e.g.*, Costinot et al., 2016; Donaldson and Hornbeck, 2016; Pellegrina, 2020). These models abstract from forward-looking behavior and lumpy adjustments to study general equilibrium effects in a tractable framework. A similar point can be made about the large literature that estimates the treatment effects of different policies used to mitigate deforestation (*e.g.* Alix-Garcia et al., 2015; Jayachandran et al., 2017) and about discrete choice approaches that capture dynamic incentives using reduced-form models (*e.g.*, Lubowski et al., 2006; Heilmayr et al., 2020). The literature focused on the Brazilian Amazon has shown that, in fact, policies implemented during the 2000s were very effective in reducing deforestation by 70% in a very short period (*e.g.*, Nepstad et al., 2014; Assunção et al., 2015; Assunção and Rocha, 2019; Burgess et al., 2019). Our results quantify the potential emission reductions and welfare implications of enhancing this set of policies, particularly through policies attached to the carbon content of the forest.

Finally, we add to the literature discussing cropland responses to prices and the economic

³This can be relevant to mitigate the effect of policies known to put pressure on deforestation in designated areas, such as infrastructure building, protected areas, or zoning (*e.g.* Asher et al., 2020; Soares-Filho et al., 2010; Nolte et al., 2013; Alix-Garcia et al., 2018; Assunção et al., 2023b; Harding et al., 2021).

⁴We find a carbon tax of \$10 per ton would preserve 95% of the carbon stored in forests outside protected areas, while Souza-Rodrigues (2019) estimate that a carbon tax of \$18.50 per ton would make farmers indifferent between producing or preserving the forest inside their properties.

environment (Chomitz and Gray, 1999; Lubowski et al., 2006; Fezzi and Bateman, 2011; Scott, 2013; Harding et al., 2021; Sant’Anna, 2024). We estimate the effects of prices on farmers’ long-run land-use choices. We find a strong substitution effect between pastureland and cropland, and a long-run cropland elasticity with respect to crop prices higher than what Scott (2013) estimates for the United States (also based on a dynamic model) and what Dominguez-Iino (2021) estimate for private properties in Brazil and Argentina (based on a static model). This highlights different land-use dynamics of a consolidated developed agricultural region – such as the United States or within delimited private properties – versus a developing agricultural frontier – such as in low- and middle-income countries or areas with weak land rights. Our results are consistent with those Sant’Anna (2024) found when studying sugarcane expansion in Brazil, using different data and estimation methods.

The paper proceeds as follows. Section 2 presents an overview of land use and deforestation in the Brazilian Amazon. Section 3 presents our model and derives the regression used to recover the model’s parameters. Section 4 describes the data used to estimate the model. Section 5 discusses the identification, estimation, and our estimates. We present the counterfactual results and welfare analysis in Section 6. We discuss the main caveats of our exercise and present extensions in Section 7. Section 8 concludes.

2 Background

We start with a brief background on the key elements of our empirical setting that guide our model. We study land use in the Legal Amazon region in Brazil, the administrative region that includes the Amazon biome and is subject to specific environmental and land use regulations. In 2000, this region had 84% forest cover, amounting to five million km^2 or 61% of the Brazilian territory (Figure D.1). After years of peak deforestation, the Brazilian government implemented the Action Plan for the Prevention and Control of Deforestation in the Legal Amazon (PPCDAm) between 2004 and 2007, creating new environmental regulations and strengthening enforcement. The government created new protected areas (indigenous land and conservation units) and toughened the penalties for environmental crimes. These conservation policies reduced deforestation (e.g., Assunção et al., 2015; Burgess et al., 2019). We focus on the period 2008-2017 under the new regulatory framework, studying unprotected areas (which account for 44% of the Legal Amazon) where cash crops are allowed.

The most important agricultural activity in the region is cattle ranching, accounting for 21% of the land use in our sample. Ranchers raise cattle in the region in extensive operations. Cattle then moves up the supply chain for finishing in a concentrated downstream

meatpacking industry (Dominguez-Iino, 2021). About 80% of the beef produced in Brazil is consumed domestically. In our sample, crops accounted for only 3% of the land use in 2008 but have steadily expanded to 4% by 2017, with soybeans and maize being the main crops (73% of cropland). Soybeans and maize production in Brazil is mainly export-oriented, with prices determined in international markets.

Geographical determinants like soil, climate, transportation costs, and other fixed land characteristics shape agricultural land-use choices (Bustos et al., 2016; Costinot et al., 2016; Pellegrina, 2020). These factors will also be important in our context, especially transportation costs. Production in the Amazon relies on a sparse road network and river waterways, with transportation costs being prohibitive in extensive areas deep in the rainforest (Souza-Rodrigues, 2019). This is especially true for cattle and beef production which relies on road networks and makes little use of waterways.

Table 1: Land Use Shares and Transitions in the Legal Amazon

	Land use 10^6 km^2 2008 (1)	Land use share 2008 (2)	Land use share 2017 (3)	Land use transitions from 2008 (row) to 2017 (column)		
				Forest (4)	Crop (5)	Pasture (6)
Forest	2.11	0.73	0.70	0.92	0.01	0.07
Crop	0.09	0.03	0.04	0.03	0.89	0.08
Pasture	0.62	0.21	0.22	0.13	0.05	0.81

Column (1) shows total land use, in million squared kilometers, for each land use classification in 2008. Columns (2) and (3) report land use shares for each category in 2008 and 2017, respectively. In columns (4) to (6), each cell indicates the share of fields transitioning from land-use row in 2008 to land-use column in 2017. Rows do not add up to one because we omit the *other* category (i.e., non-classified pixels, urban areas, and water).

Table 1 summarizes land use and land transitions in our sample of unprotected areas. Each cell in columns (4) to (6) indicates the share of fields converting from their 2008 land use in the ‘row’ to their 2017 land use in the ‘column.’ We can see that the main driver of forest cover loss in the region has been the expansion of pasture for cattle ranching. Only 1% of areas classified as forests in 2008 transitioned to crops in 2017, while an area seven times larger transitioned from forest to pasture. Forest clearing is typically done using fire, releasing the carbon stored in the vegetation with dire consequences that go beyond climate change. After clearing, preparing the land for agriculture involves sunk costs, such as removing stumps and leveling the terrain.

We leave the action of illegal loggers outside the scope of our modeling framework. Log-

ging is typically associated with forest degradation rather than deforestation (Matricardi et al., 2020) and evidence suggests that illegal logging in the Amazon region receded by the end of the 2000’s (Chimeli and Soares, 2017). Unfortunately, the lack of precise data about these activities prevents a thorough examination of those mechanisms in our context.

Forest regeneration. We also learn from transition rates that deforestation in our setting is not a one-way street. Forest regeneration is relatively common: 13% of pasture areas in 2008 were converted back to forests in 2017. The relatively high transition rates of agricultural activities to forests, although understudied, constitute a relevant phenomenon that cannot be ignored when thinking about the dynamics of land use in the Amazon.

Two exercises provide additional evidence on the extent of forest regeneration and the reliability of this measurement. First, we use other data sources to document that between 3% and 5% of the total forest area in any given year in our sample is secondary vegetation (i.e., areas where the forest is regrowing after being previously deforested). Second, we show that regeneration is related to the unsustainable use of the land. Regeneration is more likely to happen in areas with degraded pastures and, thus, less profitable for farming. That is, the very nature of extensive cattle ranching leads farmers to cease agricultural operations in some fields whenever agricultural activities become unprofitable (see, e.g., Pendrill et al., 2022). Appendix C discusses these exercises in more detail.

3 Model

We formulate a dynamic discrete choice model in which profit-maximizing agents choose how to use each plot of land every year. Agents can convert between different land uses subject to conversion costs. In this section, we present model details and derive the structural regression equation used to estimate model parameters.

3.1 Setup

The basic unit of decision in the model is a field, denoted by i . Fields are grouped in locations, denoted by m .⁵ Each field i is run by a rational agent that chooses the profit-maximizing land use. These agents may formally own, lease or just hold informal property rights over the land. We only require they are residual claimants over the net discounted cash flow of their farming operation. Agents can choose among three possible land uses $j \in J = \{crop, pasture, forest\}$. That is, they can plant cash crops, use the land as pasture

⁵In our application, a field corresponds to 30m resolution pixel from satellite imagery, while a location stands for a coarser 1km grid where individual fields are grouped.

for cattle grazing, or leave it unused, typically, covered by native vegetation. This choice is repeated every year $t = 1, 2, \dots, \infty$.

Each land use choice generates a profit flow $\pi_j(w_{mt}, \varepsilon_{imjt})$ in year t that depends on a vector of location-specific state variables $w_{mt} \in \mathbb{R}^L$ – which include observable (*e.g.*, prices, land characteristics, transportation costs) and unobservable (to the econometrician) variables – and $\varepsilon_{imjt} \in \mathbb{R}$ which are field, choice and time specific shocks unobservable to the econometrician. We assume a separable structure for the profit function:

$$\pi_j(w_{mt}, \varepsilon_{imjt}) = r_j(w_{mt}; \alpha) + \varepsilon_{imjt}, \quad (1)$$

where $r_j(\cdot; \alpha)$ is a known function up to a vector of parameters α .

Agents must pay a land conversion cost $\Phi_{jk}(w_{mt}; \varphi)$, where $j \in J$ denotes the current land use and $k \in J$ denotes the previous period land use. For instance, $\Phi_{pasture, forest}(w_{mt}; \varphi)$ denotes the cost (or benefit) from deforestation and conversion of the field to pasture.

Assumption 1 *The evolution of location-specific state variables follows a Markov process and it is conditionally independent from field-level information (decisions and characteristics) – i.e., $F(w_{m,t+1}|w_{m,t}, \varepsilon_{imjt}, j) = F(w_{m,t+1}|w_{m,t})$.*

Assumption 1 implies that field-level decisions and characteristics do not affect the evolution of market-level variables. This is consistent with the idea that agents are price takers in competitive final product markets.

Assumption 2 *Field level shocks ε_{imjt} are independent over time and choices conditional on field characteristics and location-specific state variables, with type-I extreme value distribution.*

Assumption 2 is standard in the dynamic discrete choice literature.⁶ Assumptions 1 and 2 allow us, under usual regularity conditions, to write the agent's dynamic land use choice problem with Bellman equations. The problem of an agent in period t , with land use k in period $t - 1$ is:

$$V(k, w_{mt}, \varepsilon_{imt}) = \max_{j \in J} \left\{ \Phi_{jk}(w_{mt}; \varphi) + r_j(w_{mt}; \alpha) + \varepsilon_{imjt} + \rho E [\bar{V}(j, w_{m,t+1})|w_{mt}] \right\}, \quad (2)$$

where $\bar{V}(j, w_{mt}) = E_\varepsilon [V(j, w_{mt}, \varepsilon_{imt})]$, $\varepsilon_{imt} \in \mathbb{R}^3$ is the vector of shocks ε_{imjt} for each choice $j \in J$, and ρ is the discount rate. Intuitively, in each period t , agents choose land use based

⁶This assumption implies that within a location m , we abstract from returns of scale or the effect of social interactions that would imply dependence across fields within a location. However, we do not restrict the dependence of location-specific state variables across space.

on the expected net present value of each option, which includes the one-period flow return in t and the continuation value in $t+1$. The continuation value explicitly includes the option value of different future land uses given the current choice. For example, when deciding to deforest and transition to pasture in period t , the agent accounts for the potentially lower cost of transitioning from pasture to crop compared to forest to crop in $t+1$, as well as their expectations about future returns. We denote the non-random component of equation (2) as

$$v(j, k, w_{mt}) = \Phi_{jk}(w_{mt}; \varphi) + r_j(w_{mt}; \alpha) + \rho E [\bar{V}(j, w_{m,t+1})|w_{mt}]. \quad (3)$$

We can then re-write the agent's problem as

$$V(k, w_{mt}, \varepsilon_{imt}) = \max_{j \in J} \{v(j, k, w_{mt}) + \varepsilon_{imjt}\}. \quad (4)$$

The distributional assumption on field level shocks (Assumption 2) implies the logit conditional choice probability:

$$p(j|k, w_{mt}) = \frac{\exp(v(j, k, w_{mt}))}{\sum_{j' \in J} \exp(v(j', k, w_{mt}))}, \text{ for } k, j \in J. \quad (5)$$

This is the probability a field transitions from land use k to land use j conditional on w_{mt} .

The formulation above yields the Hotz and Miller (1993) inversion:

$$\log \left(\frac{p(j|k, w_{mt})}{p(j'|k, w_{mt})} \right) = v(j, k, w_{mt}) - v(j', k, w_{mt}), \text{ for } k, j, j' \in J. \quad (6)$$

That is, the ratio of conditional choice probabilities of different alternatives is directly related to the difference between the non-random components of returns from these alternatives.

Assumption 3 $\Phi_{jj}(w_{mt}; \varphi) = 0$ for all $j \in J$ and $w_{mt} \in \mathbb{R}^L$ – i.e., there is no conversion cost if the land is not converted.

From equations (3) and (6), using Assumption 3, we follow steps similar to Scott (2013) and write an expression reminiscent of an Euler equation:

$$\begin{aligned} \log \left(\frac{p(j|k, w_{mt})}{p(k|k, w_{mt})} \right) - \rho \log \left(\frac{p(j|k, w_{m,t+1})}{p(j|j, w_{m,t+1})} \right) &= \Phi_{jk}(w_{mt}; \varphi) - \rho \Phi_{jk}(w_{m,t+1}; \varphi) + \\ &r_j(w_{mt}; \alpha) - r_k(w_{mt}; \alpha) + \eta_j^V(w_{mt}) - \eta_k^V(w_{mt}), \text{ for } j, k \in J, \end{aligned} \quad (7)$$

where $\eta_j^V(w_{mt}) = \rho(E [\bar{V}(j, w_{m,t+1})|w_{mt}] - \bar{V}(j, w_{m,t+1}))$ denotes the expectation error in continuation values (see Appendix A.1 for details). This derivation relies on the one-period

finite dependence property that holds for our model: if j is picked in $t+1$, it does not matter for future choices ($t+2$ onward) if either j or k were chosen in t . It allows us to eliminate continuation values and write an optimality condition based on choices in two consecutive periods, similar to a typical Euler equation.⁷

It will be useful now to separate the location-specific state vector w_{mt} into its observable and unobservable components. That is, $w_{mt} = (x_{mt}, \xi_{mt})$, where $x_{mt} \in \mathbb{R}^{L-3}$ is a vector of observed variables and $\xi_{mt} \in \mathbb{R}^3$ is a vector of choice specific unobserved state variables. We require $r_j(\cdot; \alpha)$ to be linear in α with an additive location and choice specific unobservable:

$$r_j(w_{mt}; \alpha) = \bar{\alpha}_j + \alpha'_j R_j(x_{mt}) + \xi_{jmt}, \text{ for } j \in J, \quad (8)$$

where $R_j(x_{mt})$ is a choice specific known function of observables, and $\bar{\alpha}_j$ is an intercept. The functional form for $R_j(\cdot)$ will be shaped by data availability.

We assume that land use transition costs are governed by a fixed, transition-specific component. Additionally, to allow for extra flexibility in deforestation costs, we permit land use transitions involving deforestation (from forest to crop or pasture) to depend on the forest's carbon stock at the location. The land use transition costs are then given by:

$$\Phi_{jk}(w_{mt}; \varphi) = \bar{\varphi}_{jk} + \varphi 1\{k = \text{forest}\} h_m, \quad (9)$$

where $1\{\cdot\}$ is the indicator function and h_m is the time-invariant potential carbon stock at location m .

Structural regression equation. Finally, we recover a regression equation by substituting (8) into (7):

$$\log \left(\frac{p(j|k, w_{mt})}{p(k|k, w_{mt})} \right) - \rho \log \left(\frac{p(j|k, w_{m,t+1})}{p(j|j, w_{m,t+1})} \right) = (1 - \rho)\bar{\varphi}_{jk} + (1 - \rho)\varphi 1\{k = \text{forest}\} h_m + \alpha'_j R_j(x_{mt}) - \alpha'_k R_k(x_{mt}) + \bar{\alpha}_j - \bar{\alpha}_k + \xi_{jmt} - \xi_{kmt} + \eta_j^V(w_{mt}) - \eta_k^V(w_{mt}), \text{ for } j, k \in J. \quad (10)$$

The left-hand side depends only on conditional choice probabilities that can be observed (estimated) directly from the data. On the right hand side, we have regressors $R_j(x_{mt})$ and $R_k(x_{mt})$, aggregate shocks ξ_{jmt} and ξ_{kmt} , and an structural error $\eta_j^V(w_{mt}) - \eta_k^V(w_{mt})$. Given our assumption that agents hold rational expectations, the structural error is the difference between expected and realized continuation value. These are true error terms with mean

⁷Aguirregabiria and Magesan (2013) formalizes the connection between the continuous choice Euler equation and the dynamic discrete choice setting using the powerful abstraction that agents choose conditional choice probabilities (which are continuous) ahead of idiosyncratic shock realizations.

zero conditional on information at t and transition-specific intercept terms.

We let the $\bar{\alpha}_j$ absorb choice-specific components that are constant across locations and time. This implies ξ_{jmt} is mean zero across locations and time. Because ξ_{jmt} and $\bar{\alpha}_j$ always appear as a sum, this is a true normalization and innocuous to any counterfactual.

To disentangle conversion costs $\bar{\varphi}_{jk}$ from $\bar{\alpha}_j$ and $\bar{\alpha}_k$, we need to assume a grounding condition. We assume that forest regeneration in our data set is driven by land left idle. Therefore, there are no costs when transitioning from pasture or crop back to forest. This is a natural assumption because the extent of active reforestation in the Amazon is minimal.

Assumption 4 *The fixed conversion cost from crop or pasture to forest is zero – i.e., $\bar{\varphi}_{forest,k} = 0$ for $k \in \{crop, pasture\}$.*

3.2 Flow of profits

We now discuss our specification of flow profits $r_j(\cdot; \alpha)$ in equation (1) for each choice of land use. These specifications are mainly context and data-driven. Our presentation here will anticipate many of the covariates we have gathered for our analysis.

Crop. In our setting, agriculture gives us a natural structure of flow profits for using the land to grow crops. Products produced in each parcel of land could be transported to destination markets and sold at market price. The net revenue from this operation is

$$(p_{ct} - z_{cm})y_{mc} + \bar{\alpha}_{crop} + \xi_{crop,m,t}, \quad (11)$$

where y_{mc} is the expected yield of crop c in location m , p_{ct} is the output price in destination markets, z_{mc} is the transportation cost from location m to destination markets, and $\bar{\alpha}_{crop} + \xi_{crop,m,t}$ is a fixed cost associated with cropland that absorbs costs with inputs, wages, and other unobserved factors that are allowed to vary across locations and time. Specifically, we allow $\xi_{crop,m,t}$ to be correlated with potential yields and transportation costs. This may be important in contexts in which transportation cost plays a major role in land use choices. Although river placement may be considered exogenous, road placement may correlate with unobserved factors affecting crop returns and land value.

We do not observe which crop is produced in each parcel. Instead, we use a weighted average of crops produced in location m 's region:

$$\tilde{r}_{mt} = \sum_{c \in \mathcal{C}} s_{cm} (p_{ct} - z_{mc}) y_{mc}, \quad (12)$$

where s_{cm} is the share of crop c in location m 's region. Thus, the net payoff for crop becomes:

$$r_{crop}(w_{mt}; \alpha) = \alpha_{crop} \tilde{r}_{mt} + \bar{\alpha}_{crop} + \xi_{crop,m,t}, \quad (13)$$

where \tilde{r}_{mt} is the only regressor measured in monetary units (in our case, Brazilian reais). We use its coefficient, α_{crop} , to give a monetary value to our counterfactuals.⁸

Pasture. A full structural model for pasture and livestock grazing is challenging given the inherently dynamic nature of cattle raising, which features an important time-to-build component. Ranchers fatten calves until they are ready for slaughter, but may adjust finishing times depending on market conditions. Decisions about breeding or buying calves also need to be made in anticipation of future market conditions. These cattle-raising dynamics may have aggregate implications for beef markets, generating the cattle cycles studied by Rosen et al. (1994). Unfortunately, there are no datasets that allow us to make clear links between our observed pixels and the quantity or age of herds. Therefore, we choose to model the return of pasture land as its capacity for cattle feeding, measured by the pasture suitability index, and our measure of transportation costs:

$$r_j(w_{mt}; \alpha) = \alpha_{j,t}^1 y_{m,j} + \alpha_{j,t}^2 d_m y_{m,j} + \bar{\alpha}_j + \xi_{j,m,t} \text{ for } j = \text{pasture}, \quad (14)$$

where d_m is road distance to port and $y_{m,pasture}$ is a measure of pasture suitability. We allow for time-varying coefficients on the pasture suitability to accommodate time-varying factors (including beef price formation) that may depend on unmodeled cattle-specific dynamics.⁹ Like agricultural products, livestock products must be transported to a destination market, so we use a structure reminiscent of the one for crops in which distance interacts with suitability. Overall, we impose less structure on pasture flow profits, being considerably more flexible than for crops.

Forest. Finally, we model the return of leaving a field in location m unused to depend on the carbon stock of native vegetation h_m in that field. So, for $j = forest$, we have:

$$r_{forest}(w_{mt}; \alpha) = \alpha_{forest} h_m + \xi_{forest,m,t}. \quad (15)$$

The coefficient α_{forest} captures the combination of two elements. First, the effect of environ-

⁸An alternative observational equivalent presentation of our model would have $\alpha_{crop} = 1$, as the regressor is already measured in reais, but would allow for a free dispersion parameter in the distribution of the logit shock.

⁹Allowing for time-varying coefficients is, as far as we know, new in the land use discrete choice literature. This flexibility might be important in our context given the concentrated downstream meatpacking industry and the domestic destination of the production (Dominguez-Iino, 2021).

mental protection policies targeted at forest preservation that are linked to forest density. It measures how much those policies help farmers internalize the value of the standing forest. Second, the private costs and benefits associated with forest density. On the cost side, higher levels of carbon stored indicate an area of dense forest that may be more susceptible to encroachment, since the property delimitation may be blurred and more costly to enforce, resulting in potential loss of property rights or other damages (see, e.g., Hornbeck, 2010). On the benefit side, preserving an area with high carbon stock may correlate with benefits such as protecting riparian forests and water springs, and avoiding soil erosion (Coad et al., 2008).

We normalize the intercept $\bar{\alpha}_{forest}$ to zero. Therefore, other costs and benefits of keeping forests that are not related to forest density will be captured by the intercepts of pasture and crop returns and by the structural error $\xi_{forest,m,t}$.

4 Data

4.1 Land use in the Brazilian Amazon

We obtain information on land use in the Amazon biome from the MapBiomas project.¹⁰ MapBiomas uses Landsat images to classify the use of each 30-meter resolution pixel in Brazil into several land use categories every year. We aggregate land use into four categories: crops, pasture, forest, and other (i.e., non-classified pixels, urban areas, and water). We exclude pixels in the other category and all protected areas from our sample.

The key element to build the dependent variable in our regression equation (10) is the conditional choice probability $p(j|k, w_{mt})$ – the probability of transitioning from land use k to j conditional on location and time. We estimate this conditional probability non-parametrically. Even in a large sample, the curse of dimensionality in field characteristics implies that a full non-parametric estimation of these conditional probabilities would be imprecise. We compute the conditional probability on the two geographical dimensions: latitude and longitude. This reduces the number of field characteristic dimensions used. We believe this is a good compromise for land use applications because all field characteristics vary smoothly over space. For a given pair of years (e.g., 2008 and 2009) and a transition (e.g., crop to pasture), we build a matrix of zeros and ones, where one indicates that a 30-meter pixel made this transition between those years. This transition matrix has many

¹⁰Project MapBiomas - Collection 4.0 of Brazilian Land Cover & Use Map Series, accessed on 20/01/2020 through the link: <http://mapbiomas.org>.

zeros, as transition rates between some pairs of land uses are low.¹¹ We then take the average of nearby pixels reducing our dataset resolution from 30 meters to 1 kilometer. Land-use decisions are highly correlated across space, so working with a coarser resolution attenuates efficiency issues arising from this spatial correlation and reduces computational costs.

We map this resolution coarsening directly into our model. A 30-meter pixel represents a field – denoted by i in our model – and a 1-kilometer pixel represents a location – denoted by m – where our suitability measures ($y_{mc}, y_{m,pasture}$), transportation variables (z_{mc}, d_m), carbon stock (h_m) and most importantly the aggregate shocks ξ_{jmt} are homogeneous. This aggregation is natural in our setting, given the resolution of the remaining variables.

Even at a 1-kilometer resolution, many locations have close to zero transition rates. Those extreme conditional choice probabilities make it impossible to compute the Hotz-Miller inversion needed for model estimation. To deal with this, we smooth the probabilities of each location m by applying a Gaussian filter to the grid of locations.¹² This technique is commonly used for image processing to blur the images and reduce noise. We provide additional details on the estimation of conditional choice probabilities in Appendix B.2. With the conditional choice probabilities in hand, we compute the dependent variable of (10), taken as given the discount rate ρ .

Satellite-based data can contain measurement errors (Alix-Garcia and Millimet, 2022; Torchiana et al., 2022). In particular, Torchiana et al. (2022) show that classification errors in the cross-section may compose large transition errors and propose a methodology to correct this type of measurement error. However, we are unable to apply this methodology. First, we do not have access to the raw (uncorrected) MapBiomass data or ground data for the whole Amazon in our period at our sample resolution. Second, it would be computationally infeasible to implement the correction on the full sample. Most importantly, MapBiomass already applies algorithms to check and correct transitions using temporal consistency rules.

4.2 Field characteristics

We now detail the different land characteristics used to model the flow profits under different uses in equations (13) to (15).

Carbon stock. We model the return of leaving the field i unused to depend on the carbon stock of native vegetation in 2000 (equation 15). Our carbon stock data comes from the

¹¹This is partially depicted in Table 1, where we highlight the low transition rates between forest to crop. There will be less persistence over longer periods than a year to year, so we need to deal with transitions with much lower values than depicted in Table 1.

¹²We set the standard error of the Gaussian distribution to 150 kilometers to eliminate most zero transitions. When applying this filter, we ignore the transition coming from pixels inside protected areas.

Woodwell Climate Research Center, which provides values for 30-meter resolution of above-ground live woody biomass that we convert to the potential of CO_2 release (Zarin et al., 2016).¹³ For exposition purposes, we will call this measure the carbon stock.¹⁴

The carbon stock data is key for our main counterfactual exercises as it gives us a measure of the location-specific social cost of deforestation. We assume all carbon is released following deforestation.¹⁵ This is motivated mostly because most of deforestation happens through slash and burn (Cochrane, 2003). Even if not burnt, the wood from cut forest decomposes fast due to forest humidity (Chambers et al., 2000). Figure 1a shows the amount of carbon stored in the forest in 2000, the first year for which we have carbon stock data. For areas deforested before 2000, our carbon stock measure will not indicate the full long-run carbon stock potential. Therefore, we restrict our sample to pixels outside protected areas that were not deforested before the year 2000, which amounts to 81% of the observations. For our sample, we treat the measure of carbon stock in each pixel as the maximum attainable carbon density that the pixel may accumulate. This implies that for our calculations, regeneration benefits under efficient forestation do not extend to 2000s levels, likely underestimating the regeneration potential in the Amazon.

Crop returns. We model the return for crops specified in equation (13). That is, the return of crop in a field in location m in year t is the weighted average of the expected revenue from different crops in location m 's region, net of transportation costs to the nearest port. We consider soy and maize as possible crops, which constitute the bulk of cash crops produced in the Amazon. The weighting of these different crops is taken by the share of each crop in m 's mesoregion¹⁶ from the 2006 Census of Agriculture sourced by the Brazilian Institute of Geography and Statistics (IBGE).

The potential yield for each crop is from the Food and Agriculture Organization's (FAO) Global-Agroecological Zones project, which provides crop-specific yield estimates at approximately 10-kilometer resolution. Those potential yields are given for scenarios differing by

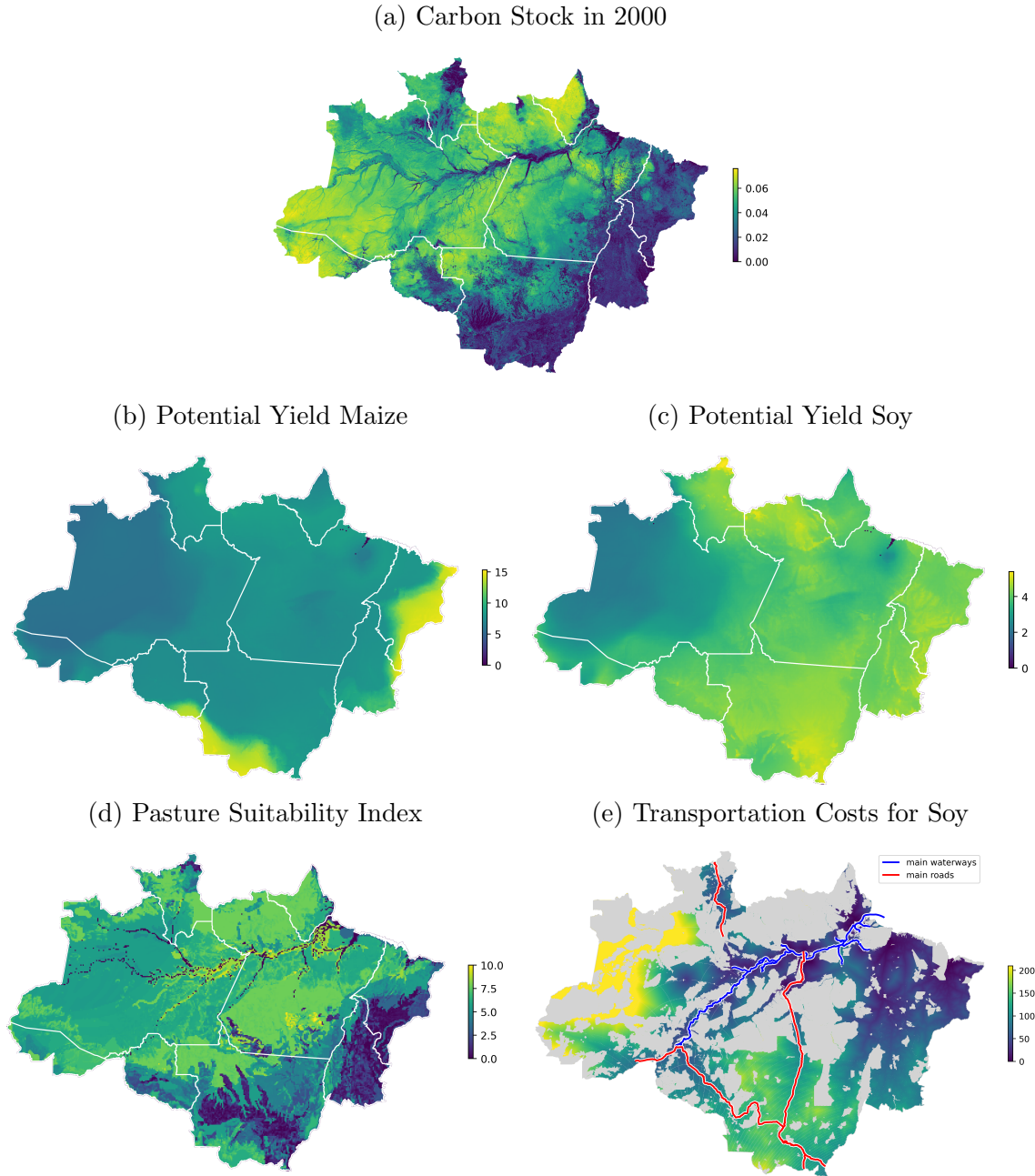
¹³We only consider aboveground biomass because: (i) about 80% of the biomass of tropical forests are aboveground (IPCC, 2019); (ii) current policy in Brazil only considers aboveground carbon, including the Amazon Fund; (iii) we have no granular and reliable data for belowground biomass, including peatland; and (iv) most types of forest clearing do not release belowground biomass (Malhi et al., 2008).

¹⁴This dataset builds on the methodology of Baccini et al. (2012). The unit in the original data is megagram Biomass per hectare. To convert biomass to CO_2 per hectare, this value must be divided by 2 – giving a measure of carbon (C) – and then multiplied by 44/12 – giving a measure of carbon dioxide (CO_2). Accessed through Global Forest Watch Climate on 02/04/2020. <https://data.globalforestwatch.org/datasets/aboveground-live-woody-biomass-density>.

¹⁵This follows the good practices from IPCC (2003) and the directives from the Brazilian Ministry of Science and Technology (MCTI, 2020).

¹⁶A mesoregion is a classification from the Brazilian Institute of Geography and Statistics (IBGE) that groups contiguous municipalities with common geographic and socioeconomic characteristics.

Figure 1: Carbon Stock, Agricultural Potential Yield, and Transportation Costs



This figure plots carbon stock density (a), measured in 10^4 tons of CO_2 per ha, the potential yield (tons per hectare) of maize (b) and soy (c), the index for pasture suitability (d) from FAO-GAEZ, and the minimum transportation costs of soybeans (e) from every pixel to the international market in Brazilian reais (R\$) per ton – the values were capped at 200 for better visualization. Values vary from blue (lower) to yellow (higher). Figure D.4 shows a histogram with the distribution of the carbon stock data.

available inputs and water sources. We use the yields of high-input, market-oriented agriculture production, and rainfed cultivation, the predominant form of production in the Brazilian

Amazon. Figure 1b-c illustrate the potential yields for maize and soy. We see substantial variation in soy suitability and greater maize suitability in the East and Southwest regions. To calculate the revenues of the potential yield, we use yearly maize and soy prices from the economic research center at the College of Agriculture Luiz de Queiroz (ESALQ).

Pasture returns. We model the location-specific return for pasture grazing by interacting potential pasture suitability with year dummies and the transportation costs to the nearest port (equation 14). We use the potential suitability index for livestock grazing from FAO illustrated in Figure 1d. Different from our potential yield measures for soy and maize, the pasture suitability index is not a cardinal measure – it is not measured directly in units of output per hectare. Given the flexible pasture returns specification, we believe this non-cardinality is not a serious limitation.

Transportation costs. We estimate the cost of transporting agricultural products from each pixel to the nearest export port. While the literature calibrates these parameters, we use a state-of-the-art, data-driven approach. This requires several steps and data sources. We provide details on the technical procedures in Appendix B.1.

We first estimate the monetary cost of transporting agricultural goods on roads. We combine georeferenced data on roads from the National Bureau of Infrastructure DNIT with internal freight costs of maize and soy collected by the Group of Research and Extension in Agroindustrial Logistics at ESALQ. For each pair of locations in the freight cost data, we compute road quality-adjusted distances for different relative transportation costs over pixels with roads (paved and unpaved) and without roads. We then regress freight costs on quality-adjusted distances using non-linear least squares, as in Donaldson (2018). This gives us the monetary cost of crossing land pixels with various transport infrastructures.

Second, we collect georeferenced data on all ports and waterways from the Ministry of Transportation to calculate transportation costs by waterways. We compute the minimum cost to ship products from every location to the nearest final port, considering bi-modal transportation using Dijkstra’s shortest path algorithm. This produces a map with the monetary cost to transport each product from each location to an international port. Figure 1e plots the transportation cost of soy.

We compute the transportation cost for soybeans and maize – $z_{m,soybeans}$ and $z_{m,maize}$ in the model. For the pasture variables, we use the quality-adjusted distance – before the transformation to a monetary value via the freight cost regression – d_m in the model.

4.3 Summary statistics

We close this section by presenting summary statistics for the main cross-section variables used to estimate the model. Table 2 shows considerable cross-sectional variation in agricultural suitability and transportation costs. This variation is important because we are interested in counterfactuals with long-run shifts in agricultural returns. In our model, a permanent increase in prices is equivalent to an increase in agricultural potential yields or a decrease in transportation costs. Thus, the cross-sectional variation in the net returns of crop and cattle grazing is key to calculating price elasticities based on the model.

Table 2: Descriptive Statistics

Variable:	Potential yield			Transportation cost		Carbon Stock
	Maize	Soy	Pasture	Maize	Soy	h_m
Model analog:	$y_{m,maize}$	$y_{m,soy}$	$y_{m,pasture}$	$z_{m,maize}$	$z_{m,soy}$	($10^4 t/ha$)
Unit:	(t/ha)	(t/ha)	(index)	(R\$/t)	(R\$/t)	
	(1)	(2)	(3)	(4)	(5)	(6)
mean	5.63	3.33	5.11	103.42	102.31	0.03
std	1.43	0.58	2.25	61.21	62.08	0.02
25%	5.13	3.12	3.91	57.14	55.37	0.01
50%	5.33	3.53	5.61	92.88	91.62	0.03
75%	5.67	3.72	6.68	137.53	136.90	0.05

This table shows descriptive statistics for the field characteristics used in the model's estimation. Transportation costs are in Brazilian reais (R\$) as of 2008, the first year we have data on transportation costs. We show variation throughout the years of the potential yield multiplied by crop prices in Table D.1. Figure D.4 shows a histogram with the distribution of the carbon stock data. Figure D.3 presents the evolution of maize and soybeans prices, highlighting that prices were stationary over our study period.

5 Identification and Estimation

We estimate the structural equation (10) which relates the conditional choice probabilities and returns of land uses in two steps. To allow for systematic differences across locations in unobservables ξ_{jmt} , we first use standard panel techniques to estimate coefficients for time-varying regressors related to crop and pasture returns. We then estimate the remaining coefficients by Ordinary Least Squares using the equation in levels. We conduct inference by block bootstrap with 1,000 iterations in a grid of 25km by 25km, explicitly allowing for dependence in ξ_{jmt} across space.

5.1 First step: Within location estimation

We take differences over time in equation (10) to eliminate the fixed location-specific component of ξ_{jmt} :

$$\Delta Y_{j,k,m,t} = \alpha_{crop} X_{j,k,m,t} + (\alpha_{pasture,t}^1 - \alpha_{pasture,t-1}^1) W_{j,k,m,t} + \Delta \zeta_{j,k,m,t}, \quad (16)$$

where the dependent variable $\Delta Y_{j,k,m,t}$ is the first difference of the dependent variable in equation (10):

$$\begin{aligned} \Delta Y_{j,k,m,t} &= \left[\log \left(\frac{p(j|k, w_{mt})}{p(k|k, w_{mt})} \right) - \rho \log \left(\frac{p(j|k, w_{m,t+1})}{p(j|j, w_{m,t+1})} \right) \right] \\ &\quad - \left[\log \left(\frac{p(j|k, w_{m,t-1})}{p(k|k, w_{m,t-1})} \right) - \rho \log \left(\frac{p(j|k, w_{mt})}{p(j|j, w_{mt})} \right) \right]. \end{aligned}$$

By estimating the model parameters accounting for location-specific fixed effects, we net out market-level unobservables that do not change in our study period, such as distance to forest core, agricultural technology, and access to electricity. The regressors $X_{j,k,m,t}$ and $W_{j,k,m,t}$ are, respectively, the returns in difference for crop and pasture defined as:

$$\begin{aligned} X_{j,k,m,t} &= \begin{cases} (\tilde{r}_{mt} - \tilde{r}_{m,t-1}) & , \text{ if } j = \text{crop and } k \neq \text{crop}, \\ -(\tilde{r}_{mt} - \tilde{r}_{m,t-1}) & , \text{ if } k = \text{crop and } j \neq \text{crop}, \\ 0 & , \text{ otherwise.} \end{cases} \\ W_{j,k,m,t} &= \begin{cases} y_{m,pasture} & , \text{ if } j = \text{pasture and } k \neq \text{pasture}, \\ -y_{m,pasture} & , \text{ if } k = \text{pasture and } j \neq \text{pasture}, \\ 0 & , \text{ otherwise.} \end{cases} \end{aligned}$$

Forest return is not in this equation because it does not vary across time. The error term is:

$$\begin{aligned} \Delta \zeta_{j,k,m,t} &= [\eta_j^V(w_{mt}) - \eta_k^V(w_{mt})] - [\eta_j^V(w_{m,t-1}) - \eta_k^V(w_{m,t-1})] \\ &\quad + [\xi_{j,m,t} - \xi_{k,m,t}] - [\xi_{j,m,t-1} - \xi_{k,m,t-1}]. \end{aligned}$$

This procedure, however, creates endogeneity in regression (16) because the error term $\eta_j^V(w_{m,t-1})$ is a difference between expected and realized values, thus correlated with \tilde{r}_{mt} . To circumvent this identification issue, we follow Anderson and Hsiao (1981) and use lagged values of returns ($\tilde{r}_{m,t-2}$) as an instrument for $X_{j,k,m,t}$.¹⁷ This is a valid instrument since

¹⁷We could, in principle, estimate the model using the Arellano and Bond (1991) estimator as Scott (2013).

Table 3: Crop Flow Profit Coefficient

Regressor	Model Parameter	Estimate
(1)	(2)	(3)
$X_{j,k,i,t}$	α_{crop}	0.392 (0.016)
$W_{j,k,i,2011}$	$\Delta\alpha_{pasture,2011}^1$	0.034 (0.001)
$W_{j,k,i,2012}$	$\Delta\alpha_{pasture,2012}^1$	-0.011 (0.001)
$W_{j,k,i,2013}$	$\Delta\alpha_{pasture,2013}^1$	-0.039 (0.002)
$W_{j,k,i,2014}$	$\Delta\alpha_{pasture,2014}^1$	0.030 (0.002)
$W_{j,k,i,2015}$	$\Delta\alpha_{pasture,2015}^1$	-0.055 (0.001)
$W_{j,k,i,2016}$	$\Delta\alpha_{pasture,2016}^1$	0.058 (0.001)

This table shows the estimates of α_{crop} obtained in the second stage regression (equation 16) using Anderson and Hsiao (1981) estimator. Column 1 reports regressors, while Column 2 displays the corresponding model parameters from Section 3.2, equations (14) and (15). Standard errors in parenthesis were computed with block bootstrap with 1,000 iterations in a grid of 25km by 25km. Number of observations: 79,478,568.

$\tilde{r}_{m,t-2}$ is information known at $t-1$, so uncorrelated with the expectational error $\eta_j^V(w_{m,t-1})$.

Prices are the only observed state variables that vary over time. So, since we take differences in \tilde{r}_{mt} , variation in prices over time helps identify this coefficient. However, this is not the sole variation in \tilde{r}_{mt} that allows the identification of the crop coefficient. In our formulation for crop return, cross-sectional variation in potential yields and crop shares magnify the price effect, generating substantial cross-sectional variation in $X_{j,k,m,t}$.¹⁸

Table 3 presents estimates for equation (16). The third column displays our baseline estimates. As expected, we estimate a positive α_{crop} coefficient, meaning that an increase in crop returns increases the likelihood of land being converted to crop. Table D.2 presents the results for the first stage, where we regress the returns variable in difference ($X_{j,k,m,t}$) on its lagged value in level ($\tilde{r}_{m,t-2}$).

The difference between the two estimators is the asymptotic efficiency. Due to our large data set – we have 79,478,568 observations in our main specification –, efficiency is not a practical problem. Moreover, the size of our data set would make it difficult to implement Arellano and Bond (1991)'s estimator.

¹⁸From equation (12), $\tilde{r}_{mt} - \tilde{r}_{m,t-1} = \sum_{c \in C} s_{cm} y_{mc} (p_{ct} - p_{c,t-1})$, which will vary in the cross-section of locations m . Figure D.2 displays the cross-sectional variation in crop return difference.

5.2 Second step: Estimation in levels

We use the estimated $\hat{\alpha}_{crop}$ and $\Delta\hat{\alpha}_{pasture,t}^1$ to estimate the remaining parameters in equation (10) in levels by ordinary least squares. Table 4 shows the results. The variables composing the pasture return do not have a direct structural interpretation, as those variables are used to flexibly model the livestock grazing returns.

Carbon stock coefficient. The coefficient on the field's carbon stock has an economic interpretation. Its estimated positive value indicates that a higher carbon stock in a plot decreases the likelihood of conversion to other uses. Monetizing the carbon stock coefficient – *i.e.*, dividing it by $\hat{\alpha}_{crop}$ – yields an estimated farmers' perceived value of preserving carbon in the forest of R\\$ 1.126 per ton of CO_2 per year.¹⁹ This value rationalizes land use choices in the data, reflecting the economic and regulatory incentives farmers face. It is substantially smaller than the annualized value of most estimates of the social value of carbon, starting at R\\$7.6 (Nordhaus, 2014) and centered around R\\$20.6 (EPA, 2016) per ton of CO_2 per year.²⁰

Transition costs. We recover the fixed conversion costs, $\bar{\varphi}_{jk}$, and choice-specific constants, $\bar{\alpha}_j$, from the transition-specific intercepts of the equation (7) in levels.²¹ Table 4 shows the recovered parameters. We estimate that it is more costly to convert denser forest plots. Each ton of CO_2 in the forest increases the deforestation cost by R\\$10.67 per hectare. That is, for the average forested field (carbon density of 300t/ha), about 20% of the conversion cost from forest to pasture is due to forest density. The fixed conversion costs are all internally consistent. The results show that the cost of clearing forests to grow crops exceeds the cost of clearing for pasture. This aligns with the intuition that preparing land for agriculture requires more investments than preparing land for pasture.

6 Counterfactuals

In this section, we use the estimated model to assess carbon-efficient forest cover and discuss alternative policies to mitigate inefficient emissions. Our goal is to evaluate how policies

¹⁹Carbon stock, h_m , is measured in $10^4 t/ha$, while crop return, \tilde{r}_{mt} , in $10^3 R\$/ha$. Thus, the ratio $\alpha_{forest}/\alpha_{crop}$ is measured in $10t/R\$$. We then divide by 10 the corresponding 11.26 estimate in column 4 of Table 4 for a measure in $R\$/t$.

²⁰We calculate the annuity equivalent to the social cost of carbon of US\\$ 18.50/ton (Nordhaus, 2014) and US\\$ 50/ton (EPA, 2016) using a 10% annual interest rate and the December 2019 exchange rate of \\$0.243.

²¹We have six transition-specific intercepts $\tau_{j,k}$ for $j \neq k$ related to model parameters through the system of equations:

$$\tau_{j,k} = (1 - \rho)\bar{\varphi}_{jk} + \bar{\alpha}_j - \bar{\alpha}_k, \text{ for } j \neq k.$$

Normalizing $\bar{\alpha}_{forest} = 0$ and using Assumption 4 leaves four $\bar{\varphi}_{jk}$ and two $\bar{\alpha}_j$ free, which the system justly identifies.

Table 4: Forest and Pasture Flow Profits Coefficients

Regressor (1)	Model Parameter (2)	Estimate (3)	$/\alpha_{crop}$ (4)
h_m	α_{forest}	4.41 (0.32)	11.26 (1.24)
$h_m \mathbf{1}\{k = forest\}$	$(1 - \rho)\varphi$	-4.18 (0.09)	-10.67 (0.50)
$W_{j,k,m}$	$\alpha_{pasture, 2011}^1$	0.06 (0.01)	-
$W_{j,k,m} d_m$	$\alpha_{pasture}^2$	-0.001 (0.01)	-
Intercepts			
	$(1 - \rho)\Phi(past, forest)$	-0.46 (0.01)	-1.18 (0.05)
	$(1 - \rho)\Phi(crop, forest)$	-0.81 (0.01)	-2.06 (0.08)
	$(1 - \rho)\Phi(crop, past)$	-0.60 (0.01)	-1.52 (0.06)
	$(1 - \rho)\Phi(past, crop)$	-0.20 (0.01)	-0.51 (0.02)
	$\bar{\alpha}_{pasture}$	0.13 (0.01)	0.32 (0.02)
	$\bar{\alpha}_{crop}$	-0.66 (0.04)	-1.68 (0.04)

This table presents the OLS estimates of equation (10), using $\hat{\alpha}_{crop}$ and $\Delta\alpha_{pasture,t}^1$ estimated in equation (16) using Anderson and Hsiao (1981). Column 1 reports regressors, while Column 2 displays the corresponding model parameters from Section 3.2, equations (14) and (15). Standard errors in parenthesis were computed with block bootstrap with 1,000 iterations in a grid of 25km by 25km. Number of observations: 79,478,568.

can shape long-run land use under current market conditions. To that end, we use the business-as-usual land use path as the benchmark to compare all policy counterfactuals.

Technically, the value function for each scenario is the key ingredient for computing the counterfactual conditional choice probabilities (CCPs) using equation (5). Numerical computation of the value function is slowed down by the size of the state space and requires knowledge of unspecified transitions for state variables.²² We make a simplification when computing the counterfactuals: we remove all uncertainty about location-specific state variables (w_{mt}) by setting $w_m = \frac{1}{T} \sum_t w_{mt}$.²³ The logit errors assumption implies that the

²²Estimation is performed without solving for the value function, a convenient feature shared by commonly used dynamic discrete choice methods (Hotz and Miller, 1993; Aguirregabiria and Mira, 2007; Scott, 2013; Kalouptsidi et al., 2021).

²³Underlying market conditions can and most likely will evolve over the decades. We did not pursue the

integrated Bellman equation has a convenient expression:

$$\bar{V}(k, w_m) = \log \left(\sum_{j \in J} \exp (\Phi_{jk}(w_m; \varphi) + r_j(w_m; \alpha) + \rho \bar{V}(j, w_m)) \right) + \gamma, \quad (17)$$

where γ is the Euler constant.

After computing $\bar{V}(j, w_m)$ by iteration, we use equations (3) and (5) to compute the CCPs. We then compute the invariant distribution for each location m , giving the steady-state probability of a pixel in m being in a specific state: $A_m(j, w_m)$. Aggregating across locations, we obtain the total steady-state land use, which we call $A(j, w)$, where $w = \{w_m\}_m$. This object is the basis for our counterfactual exercises.

6.1 Long-run effects of higher agricultural prices

In our first counterfactual exercise, we assess how agricultural price variations affect land use and carbon release. Although indirectly linked to our main research questions, this exercise helps situate our results in the broader literature. We compare the steady-state land use with (\tilde{w}) and without (w) a $100 \cdot \Delta\%$ price change and compute a long-run elasticity of land use with respect to agricultural prices:

$$\partial_{j,\Delta} = \frac{A(j, \tilde{w}) - A(j, w)}{A(j, w)} \frac{1}{\Delta}. \quad (18)$$

Table 5 Panel A reports land use elasticities with respect to crop prices. We estimate an own land-use price elasticity of 6.6 for cropland (column 2). This is high compared to the evidence for the US (Scott, 2013), but in line with similar estimates for Brazilian agriculture (Sant'Anna, 2024). Although the pasture cross-elasticity with respect to crop price is relatively high (-0.25), most cropland increase comes from forests. We find a forest cover elasticity with respect to crop prices of -0.42. These results align with literature arguing market conditions increase agriculture's pressure on forest land in areas with non-consolidated agriculture frontiers, as common in countries with tropical forests.

In Table 5 column 4, we compute the price increase effect on carbon release, assuming all aboveground biomass carbon stock is released by deforestation. We sum the carbon stock of plots weighted by their probability of converting from forest to other uses. We estimate a carbon-released elasticity with respect to crop prices of 0.13. This means a 10% crop price

alternative assumption of explicitly modeling the future trajectory of prices (including their volatility) from 2017 onwards because forecasting the evolution of prices over the next century would be highly speculative.

Table 5: Long-run Land Use Elasticities with Respect to Crop and Cattle Prices

	Forest Cover (1)	Crop Area (2)	Pasture Area (3)	Carbon Released (4)
Panel A. Crop price elasticities				
-0.42 (0.03)	6.60 (0.15)	-0.25 (0.01)	0.13 (0.01)	
Panel B. Cattle price elasticities				
-1.66 (0.05)	-0.44 (0.01)	1.43 (0.05)	1.82 (0.08)	

This table presents the long-run elasticity of forest cover, crop area, pasture area, and carbon released with respect to crop price (*Panel A*) and with respect to cattle price (*Panel B*). Elasticities calculated with $\Delta = 10\%$ (eq. 18) price increase. Standard errors in parenthesis were computed with block bootstrap with 1,000 iterations in a grid of 25km by 25km.

increase results in an additional 0.5 gigaton of CO_2 released in the steady state, amounting to \$25 billion of costs at a \$50/ton social cost of carbon (EPA, 2016).

Table 5 Panel B reports land use elasticities with respect to cattle prices. We estimate a positive own land-use price elasticity (column 3), but smaller than the cropland own price elasticity. Although some cropland converts to pastureland (cross elasticity -0.44), the main change in land use is forest conversion to pasture, with cross elasticities of -1.66 for forest cover and 1.82 for carbon release. These elasticities are substantially larger than crop price cross-elasticities, suggesting cattle market changes impact forests more than crop markets.

To illustrate the importance of considering a dynamic model featuring forward-looking agents, we re-estimate the model and elasticities assuming myopic agents (discount factor $\rho = 0$). Intuitively, static models capture only the short-run relation between returns and land use, which understates long-run responses to permanent changes in returns once forward-looking behavior is considered. As expected, own-price land use elasticities are reduced without forward-looking behavior: the forest cover elasticities with respect to crop and pasture prices drop to -0.14 and -0.47, respectively. These results suggest ignoring forward-looking behavior would underestimate agricultural prices' effect on deforestation. These myopic estimates are remarkably similar to Harding et al. (2021), which estimate a deforestation elasticity with respect to an agricultural price index of 0.47 over 2004–2013.²⁴

²⁴The elasticities reported in Table 5, calculated from aggregate land-use outcomes, represent a weighted average of millions of location-specific acreage elasticities. However, elasticities will differ for each location because they depend directly on agricultural potential yields, transportation costs, and pasture suitability, which all vary across locations. Figure D.5 presents histograms of elasticities by location, highlighting the substantial heterogeneity.

6.2 Efficient land use

In our model, the socially efficient forest cover is the one in which agents fully internalize the externalities associated with deforestation when making land-use choices. In our main counterfactual exercise, we quantify Amazon’s carbon-efficient conservation in the steady state when agents internalize the social cost of carbon stored in each forest plot. We do so by equating agents’ private perceived value of the carbon stored in the forest to the social cost of carbon of \$50 per ton of CO_2 .

We calculate that the steady-state efficient land use under a social cost of carbon of \$50 per ton would preserve 99.7% of the carbon stock and 97% of the forest cover in our sample (i.e., pixels outside protected areas that were not deforested by 2000). With 99.7% of the carbon stock already preserved when the perceived value is \$50 per ton, any higher value for the social cost of carbon would not yield meaningful additional conservation. In comparison, in the business-as-usual (BAU) steady state, only 51% of the carbon stock would be preserved. The efficient land use would result in 42 billion fewer tons of CO_2 released into the atmosphere relative to the BAU steady state (95% confidence interval: 39 to 45).²⁵ This corresponds to an additional 1,186,216 km^2 of forest cover relative to the BAU (95% confidence interval: 1,130,542 to 1,241,889).

We can benchmark the magnitudes of our estimates relative to the deforestation dynamics over the last twenty years. Hansen et al. (2013) forest loss data shows that around 565,343 km^2 was deforested in the Brazilian Amazon between 2001 and 2019. De Azevedo et al. (2018) calculates that land-use change in the Brazilian Amazon in this period released 20 billion tons of CO_2 . Thus, achieving the additional 1.1 million km^2 of forest cover and preserving 42 billion tons of CO_2 in the efficient steady state would require ceasing the current deforestation pattern for the next four decades. Alternatively, it would entail regenerating most of the deforestation over the last twenty years and stopping deforestation for the next twenty years. In sum, implementing the first-best land use is a Herculean task.

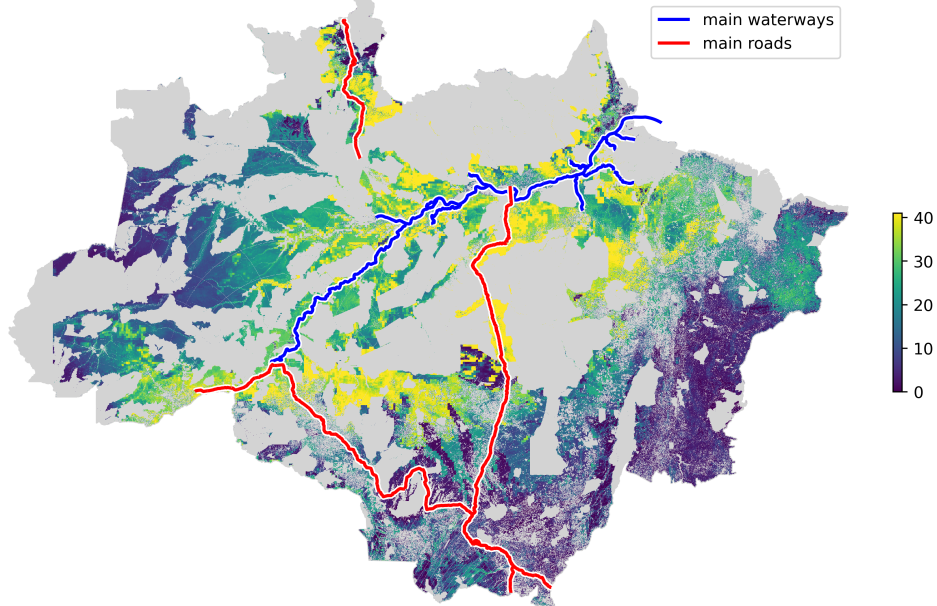
We use the spatial granularity of the data to map the pixels in which the inefficient loss of carbon would be more severe. Figure 2 displays the excess of emissions in the BAU relative to efficiency in each location. The difference between efficient and BAU carbon holdings reaches up to 40,000 tons of CO_2 per km^2 in some locations, a social loss of \$2 million per

²⁵For each location m , we compute the steady-state ‘forest’ land use probabilities in both BAU and efficient scenarios and assess excess emissions:

$$\Delta CO2_m = (A_m(forest, w_m^*) - A_m(forest, w_m)) h_m,$$

where $A_m(forest, w_m^*)$ and $A_m(forest, w_m)$ denote the steady-state probability of forest, respectively, in the efficient and BAU scenarios. Total emissions are the sum of $\Delta CO2_m$ across all locations.

Figure 2: Geographical Distribution of Inefficient Emissions in Steady State



This map displays emissions in the BAU scenario in excess of emissions in the efficient scenario (perceived carbon value of \$50) for each pixel measured in $10^3 t CO_2/km^2$.

km^2 . Those areas are especially around the main waterways and roads in the state of Pará. This large gap is due to a combination of high carbon density – which drives up efficient forest cover – and high agricultural profitability, especially because of low transportation costs – which drives forest cover down in BAU. Meanwhile, darker regions represent places in which the BAU is closer to efficiency. Those are areas with small carbon stock (on the Amazonian fringe) in the states of Mato Grosso and Tocantins, where agriculture is also more profitable. There are also low gap areas in the far west, where even though carbon stock is high, transportation costs are prohibitive. This heat map can be a useful tool for the design of cost-effective targeted conservation policies.

Because our model allows for land use transitions from pasture or crops back to forest, these long-run gaps stem from differences in deforestation and regeneration dynamics. However, primary and secondary forests provide distinct environmental services, particularly for biodiversity (Liang et al., 2022). We then investigate forest regeneration’s role in the steady-state paths.

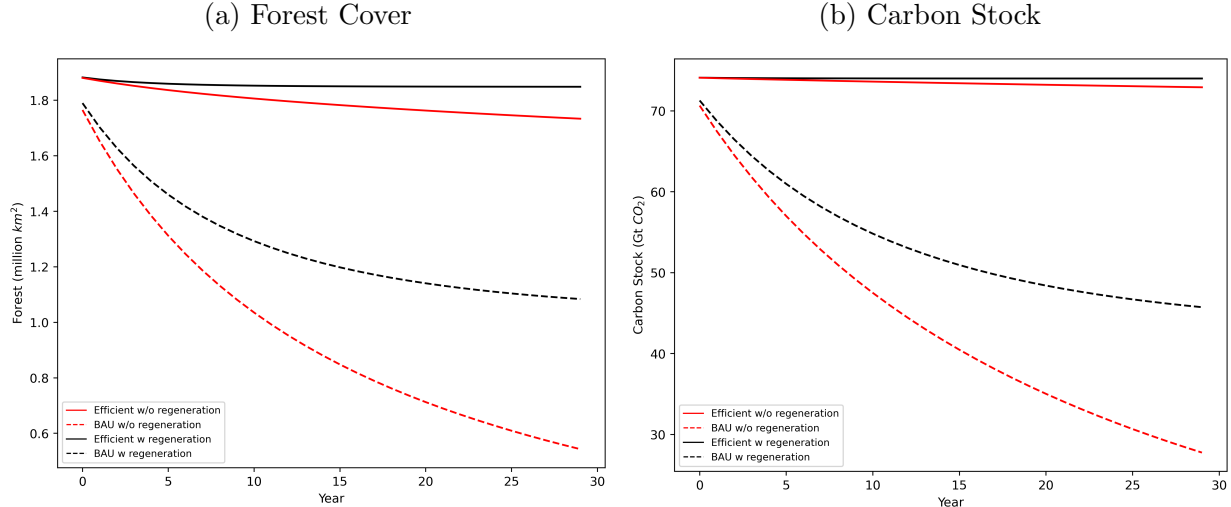
Figure 3 plots the forest cover and carbon stock dynamics for the efficient and BAU scenarios considering models with and without forest regeneration. We start in year 0 with observed 2017 land use in each location (the last year in the sample). We then track land use evolution implied by steady-state transitions for the efficient and BAU scenarios. We assess regeneration’s role by tracking forest cover and carbon stock with regeneration (our

baseline) and without (i.e., only accounting for 2017 primary forests).

Figure 3 shows that forest regeneration has little impact on the forest dynamics in efficient scenarios (solid lines). When we compare the black lines (model with regeneration) with the red lines (model without regeneration), we see that most of the primary forests are preserved in the efficient scenario, especially those with high carbon density.

However, we see that forest regeneration plays a substantial role in the BAU land use path (dashed lines). For instance, excluding forest regeneration increases the gap between efficient and BAU by 42% for forest and carbon in 15 years from 2017. This likely reflects the region’s inherent land use dynamics, with fields used until exhausted and abandoned. As we saw in Table 1, about 13% of pasture land in 2007 reverted back to secondary forest ten years later. Thus, not accounting for regeneration in our model has implications for the size and speed of divergence between the BAU and the efficient scenarios. Figure 3b shows that the emissions gaps (the difference between the solid and dashed lines) grow faster in the model without regeneration.

Figure 3: Evolution of forest cover and carbon stock

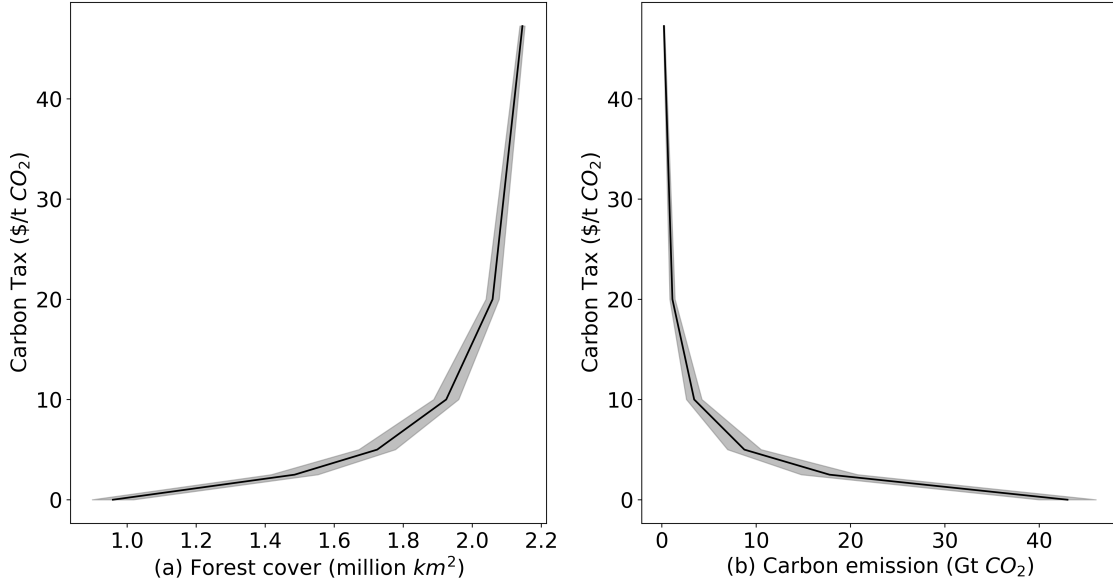


These figures show the paths of aggregate forest cover and carbon stock starting from 2017, the last year in our sample, under BAU and efficient steady-state transitions. In each figure, we plot the paths accounting for forest regeneration (our baseline exercise) and without forest regeneration, in which case we only track forest cover and carbon from forests standing in 2017.

6.3 Preserving the forest through carbon tax

We now consider how a carbon tax based on the carbon content of the land could shape farmers’ incentives and promote forest conservation. Abstracting from other externalities, a

Figure 4: Forest Cover and Carbon Emissions by Carbon Taxes



This figure shows the steady state forest cover (a) and carbon emissions (b) for different values of a carbon tax. Our baseline perceived carbon value implied by the model estimates is \$2.74 /t CO_2 . Here, we consider carbon taxes added to the baseline perceived value of carbon. The gray shaded area shows the 95% confidence interval computed using block bootstrap with 1,000 iterations for a grid of 25km by 25km.

carbon tax is the first-best policy instrument and implements the efficient long-run land use if it equates the perceived carbon return to its social value. In our discrete choice setting, a carbon tax on non-forest land use generates the same incentives as a flow of Payments for Ecosystem Services (PES) for preserving the carbon in the forest, instead of payment for forest area preserved (as in Alix-Garcia et al., 2015; Jayachandran et al., 2017; Wong et al., 2019). Thus, in this set of counterfactuals, we increase the perceived return of preserving carbon in the forest α_{forest} . We interpret the present value of this flow as a carbon tax that can be compared to current measures of the social cost of carbon. We can also interpret the increase in the perceived value of carbon as driven by stronger enforcement of environmental policies – such as using remote sensing data (Assunção et al., 2023a) or rural registries to increase compliance (Alix-Garcia et al., 2018) – as a carbon tax in our model.

We calculate steady-state land use in different scenarios considering the inclusion of carbon taxes ranging from \$0/ton to \$47.26/ton, the tax that implements the efficient land use.²⁶ Figure 4 (and Table D.3) reports the results. The figure on the left shows the amount of forest cover (on the horizontal axis) under different carbon taxes (on the vertical axis),

²⁶Our estimates imply a flow carbon return of R\$1.126/t CO_2 . Converting to present value (dividing by $1 - \rho = 0.1$) and converting to USD (exchange rate of \$0.243 from Dec 2019) yields a present value of \$2.74/t CO_2 . Thus, a \$47.26 tax plus \$2.74 equates the carbon value to the social cost of carbon of \$50/t CO_2 .

and the figure on the right shows the amount of carbon released for different values of a carbon tax. The main lesson from this figure is that there is a strong non-linearity in the amount of carbon release implied by carbon taxes, with relatively small carbon taxes closing a substantial share of the gap between the BAU and efficient forestation. For example, a carbon tax of \$2.5/ton would preserve 25 billion tons of CO_2 (and 526 thousand km^2), which amounts to 60% [=25/42] of the efficient scenario carbon savings. A carbon tax of only \$10/ton would already preserve 95% [=40/42] of the efficient carbon stock. This convexity is intuitive: preserving carbon is cheaper deeper in the forest, where carbon stock and transportation costs are higher. As the marginal preserved land gets closer to the agricultural frontier (with lower transportation costs), preserving carbon becomes increasingly costly. A second intuition for this convexity is that land is the main input for expanding cattle ranching, so relatively small increases in the perceived cost of deforestation represent a substantial increase in the cost structure of expanding pastureland.

Figure 4b also shows that virtually all conservation gains are achieved with carbon taxes under \$10/ton, which is cheaper than most mitigation strategies based on deforestation reduction with the potential of reducing emissions over 2 billion tons of CO_2 and cheaper than almost all other mitigation strategies based on agriculture, forestry, and other land uses as estimated by the IPCC (Rogelj et al., 2018, Figure TS.23).²⁷ This value is smaller than previous estimates from Souza-Rodrigues (2019) that finds that a carbon tax of \$18.50/ton would make farmers in the Amazon indifferent between producing or preserving the forest. Two main reasons may reconcile the difference between the two estimates. First, Souza-Rodrigues (2019) studies deforestation inside private properties using census data collected around 2005/2006, before the complete roll-out of environmental policies introduced in the Amazon under PPCDAm. We study deforestation in the whole unprotected Amazon after all PPCDAm policies were in place. The stronger policies likely made deforestation more costly, reducing the additional incentives needed for farmers to preserve forests on their land. Second, Souza-Rodrigues (2019) estimates a static model, which tends to underestimate land use elasticities compared to dynamic models like ours (see our discussion in Section 6.1). Although the value of \$10/ton is small compared with the previous literature, it is greater than the current value used for the Amazon Fund, a REDD+ mechanism that compensates Brazil for deforestation reductions at the price of \$5/ton.

²⁷While comparing our estimates with the IPCC's is useful, we are comparing results from fundamentally different methods and scopes. Rogelj et al. (2018) compiles mitigation costs across various sectors of the economy for the whole world using diverse methodologies, from general computable models to expert surveys.

6.4 Preserving the forest through taxes on cattle ranching

We now assess the potential of excise taxes on cattle ranching and crops to promote forest conservation. Market interventions, such as international tariffs (Abman and Lundberg, 2020; Hsiao, 2021) or bans on goods produced in areas under deforestation pressure (e.g., Nepstad et al., 2014; Harding et al., 2021), could potentially be used to de-incentivize deforestation. Such taxes are second-best policy instruments to address inefficient carbon emissions from deforestation. We, therefore, compute the steady-state land use under scenarios where agents are subject to taxes on cattle or crop goods – i.e. an *ad valorem* tax on the return of cattle ranching or crops.

Figure 5 displays the results of different tax levels on the return of cattle ranching (vertical axis) on forest cover (a) and carbon emissions (b). We find that the relationship between cattle taxes and carbon emissions is also convex, but not as much as carbon taxes. Figure 5b shows that relatively smaller taxes, such as a 20% rate, can save about 15.8 billion tons of CO_2 . A 60% tax on cattle is necessary to save the 34 billion tons of CO_2 saved under a \$5/ton carbon tax – marked with a vertical dashed line in the figure. We see a similar pattern in Figure 5a that displays the amount of forest cover for each level of a cattle tax. It shows that a 50% tax on cattle induces the same extent of forest cover in the steady state as that implied by the \$5/ton carbon tax. We also experimented with a tax on crops, but we found that it produced only marginal changes in carbon emissions.

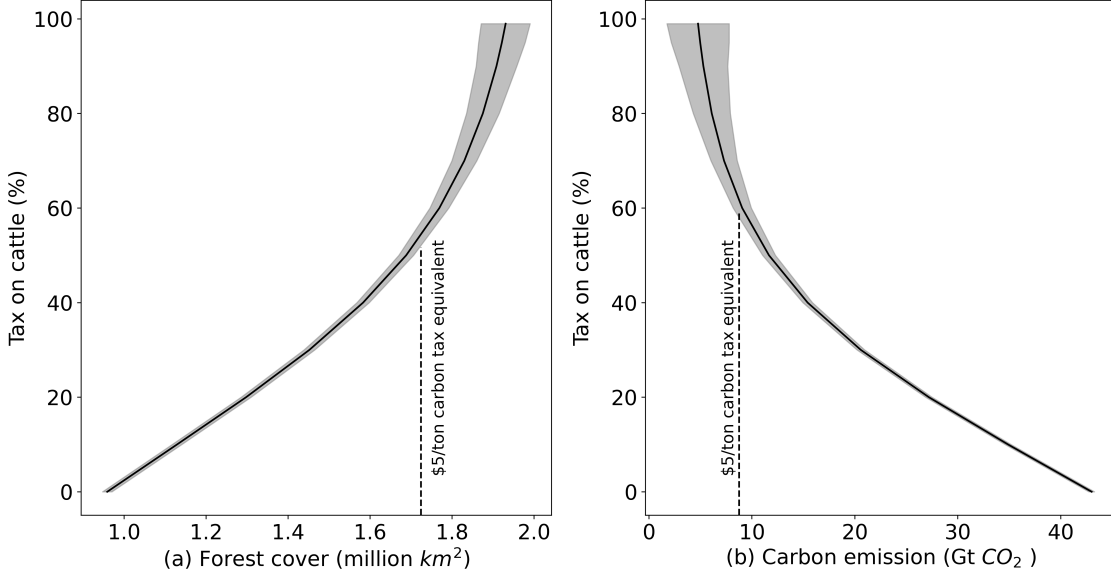
In sum, the low productivity economic activities currently in place in the region and the large amounts of carbon stored in the forest make even small increases in the stringency of environmental policies (i.e. small carbon taxes) highly effective in moving the Amazon closer to the efficient forest cover. On the other hand, current small opportunity costs of preserving the forest make small returns from deforestation, such as converting to extensive cattle ranching, privately economically attractive. Thus, only large excise taxes can sufficiently disincentivize forest conversion to mitigate inefficient carbon emissions from deforestation.

6.5 Welfare

So far we have studied the implications of first- and second-best policy instruments – the carbon and cattle taxes – for carbon emissions and forest cover. While these policies are effective in preserving carbon in the forest, they also impose losses on farmers' private profits. Next, we perform a complete welfare examination, analyzing the trade-off between private profits and the social cost of deforestation emissions under different policy instruments.

We address two related challenges to conduct this welfare analysis in our setting. First,

Figure 5: Effects of a Cattle Tax on Forest Cover and Carbon Released



This figure shows forest cover (a) and carbon emissions from deforestation (b) for different levels of excise taxes on cattle ranching. Dashed lines highlight forest cover (a) and carbon emissions (b) that would follow from a \$5/ton carbon tax for comparison across policy exercises. The gray shaded area shows the 95% confidence interval computed by using block bootstrap with 1,000 iterations for a grid of 25km by 25km.

our model is derived and estimated from the perspective of private farmers. Thus, we must first extend the dynamic model to incorporate the social benefit of carbon holdings. Second, in our dynamic environment, a policy will affect the immediate flow returns of different land-use choices and their continuation values. Although these challenges could make the evaluation of social welfare computationally cumbersome, we show in Appendix A.2 that we can analytically decompose the social welfare in location m as

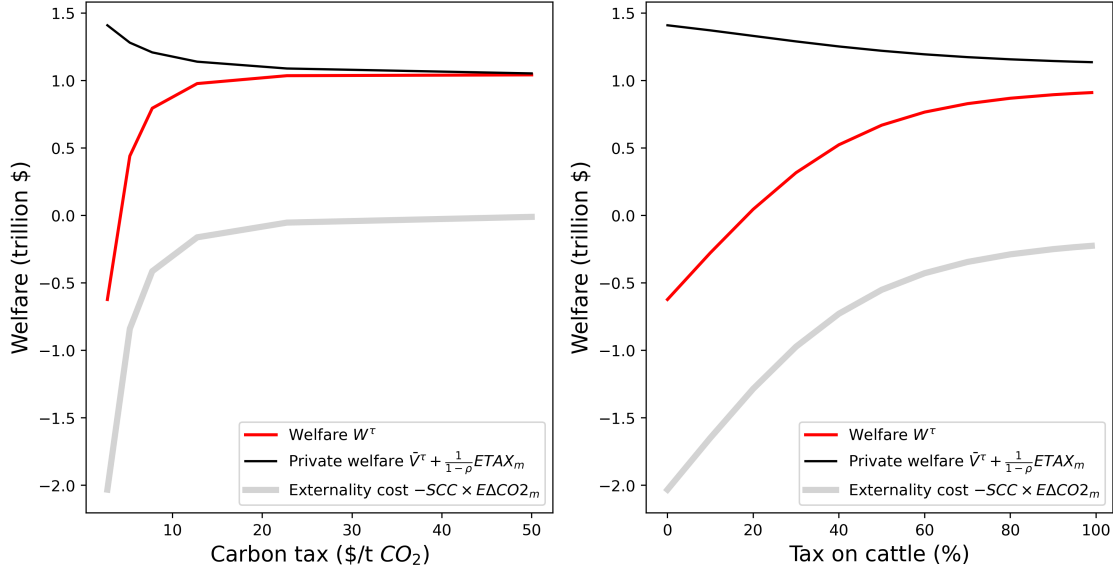
$$W^\tau(w_m) = \bar{V}^\tau(w_m) + \frac{1}{1-\rho} ETAX_m - SCC \times E\Delta CO2_m, \quad (19)$$

where $W^\tau(w_m)$ is the social welfare, $\bar{V}^\tau(w_m)$ is the private integrated steady-state value function (expression (17) integrated over initial land-uses), $ETAX_m$ is the steady-state expected tax payment, SCC is the non-internalized social cost of carbon, and $E\Delta CO2_m$ is the steady-state expected carbon emissions. The social welfare is thus the sum of the present value of private profits before tax payments discounted by the social cost of expected deforestation.²⁸ This decomposition is both informative and convenient as it decomposes welfare

²⁸Expressing the present value of private profits before tax payments is interesting because this measure is invariant to choice-equivalent policy implementations. For instance, we have discussed how a carbon tax is equivalent to a carbon-based forest PES scheme in our model, but they have different implications for private profits net of taxes. Using a gross measure of profits avoids this ambiguity.

in terms that we have either already calculated or can easily compute.

Figure 6: Welfare from carbon and cattle taxes



Social welfare from (a) the carbon tax policy instrument and (b) the cattle tax *ad-valorem* tax. The welfare on the y-axis is scaled to represent the fraction of the welfare gap between the efficient and BAU scenarios captured by each policy design. The welfare notation in the legends follows the equation (19).

Figure 6a displays social welfare and its decomposition into gross private profits and externality cost for different carbon tax levels. We identify a few key takeaways from our welfare analysis. First, we compute that the welfare loss between the BAU (carbon tax = 0) and the efficient (carbon tax = 47.26) land use paths is approximately 1.66 trillion dollars. We use this welfare analysis to decompose the welfare gains into the cost of inefficient emissions rebated (2.02 trillion dollars) minus the loss in foregone private profits (356 billion dollars). That is, for each dollar lost in private profits, there are corrective gains over fivefold, underscoring the sizable welfare benefits of addressing the externality.

Second, Figure 6a shows the welfare decomposition for the entire carbon tax schedule. It indicates a strong non-linearity in the welfare gains from the carbon tax, with small carbon taxes already capturing most of the welfare gains from this first-best policy. These gains are predominantly driven by the substantial reduction of the externality for carbon tax values under \$15/ton of CO_2 , as discussed previously.

Third, we compare the welfare gains of using first- and second-best policies. Figure 6b shows the welfare decomposition for different tax levels on the return of cattle. It shows that the second best policy in this case – i.e, the cattle tax that maximizes welfare – is a 100% tax on the returns of cattle. Our analysis shows that the second-best policy achieves

87% of the first-best welfare gains. Again, this is predominantly driven by the second-best policy implementing substantial reductions in emissions (about 1.8 trillion dollars). The loss in private profits is smaller in the second-best policy (273 billion dollars), as a cattle tax distorts land-use decisions in favor of forests but also in favor of crops. Moreover, the cattle tax shifts land-use returns away from pasture even in areas with low carbon density and high pasture profitability. Additionally, the excise tax on pasture still implements more crop planting in the Amazon than is socially optimal.

7 Caveats and extensions

Our analysis relied on assumptions and simplifications that may impact our conclusions. In this section, we discuss the main caveats when interpreting our results and present extensions.

7.1 Tipping points

When computing the social cost of deforestation, we only look at carbon emissions from land-use changes. This approach does not account for other externalities associated with deforestation. The Amazon forest is part of an ecosystem of potential tipping points with global consequences (McKay et al., 2022). As the forest generates a significant portion of its own rainfall (Spracklen et al., 2012; Staal et al., 2018), researchers have hypothesized that there exists a point of no return in deforestation, in which the rainforest cannot produce the humidity the ecosystem requires. Once deforestation crosses an estimated threshold of 40%, the forest could enter a dieback path, releasing hundreds of billions of tons of CO_2 into the atmosphere (Nobre et al., 1991; Sampaio et al., 2007; Franklin Jr and Pindyck, 2018). Recent literature has evolved to discuss the existence of local tipping points, where significant portions of the forest could cross the tipping point independently, even if the entire ecosystem does not (Gatti et al., 2021; Flores et al., 2024). This possibility underscores the importance of understanding forest dynamics at a high spatial resolution to develop environmental policies, especially given the considerable heterogeneity in the importance of different regions for the forest's stability (Araujo et al., 2023). Furthermore, a framework for forest regeneration is essential to address any tipping points that may have been crossed.

In our long-run BAU steady state, we have deforestation of 57% of our sample, which does not include protected areas. Assuming that in the long run all existing protected areas remain intact and there is no regeneration of fields deforested before 2000, total deforestation of the Amazon in the BAU steady state would be 31%, still short of the 40% tipping point.

However, this result depends on the preservation of protected areas, which is crucial to avoid long-term permanent changes to the biome (Soares-Filho et al., 2006, 2010).²⁹

All these unmodeled effects are potentially big, but we know of no study explicitly computing social costs arising from these effects that we could directly apply to our setting. Therefore, we decided to take a conservative approach of only factoring in social costs related to the release of carbon stored in the forest. However, we conjecture that these unaccounted-for externalities are all negative, which would make the optimal forest gap even larger if we explicitly factored them in.

7.2 Equilibrium effects and trade

In our analysis so far, we assume there are no equilibrium price effects when switching from BAU land use to efficient land use. This is valid, for instance, if the agricultural commodities are traded internationally and this region represents a small share of the supply,³⁰ being insufficient to affect world prices. Alternatively, if 100% of the beef production that used to be in the Amazon moves elsewhere in the world without affecting prices. However, if these conditions are not valid, an efficient carbon tax on deforestation or a tax on beef would decrease the supply of these commodities and push world prices up, decreasing the expected policy effects on deforestation in the Amazon but also mitigating potential “leakage” effects elsewhere.

We consider a simple world beef market supply and demand model and investigate the equilibrium consequences of setting land use in the Amazon to the efficient level.³¹ This model suggests a small 4.16% world beef price increase from implementing our efficient land use in the Amazon. This price increase could partially offset the decrease in deforestation by increasing acreage as we move to a new market equilibrium, as well as harming consumers worldwide. Given our estimated cattle supply elasticity of 1.43, this acreage offset would be limited to 5.9% of the cattle grazing area. Because only 2% of the region is cropland and a small share of Brazilian soybeans are harvested in the Amazon, the equilibrium effects for crops would be even smaller.

²⁹Our model is not designed to project land use in these areas. While we acknowledge that the assumption that protected areas will be preserved is quite strong, any other assumption on the long-run trends of land use in these areas would be outside the model and, therefore, similarly strong.

³⁰In 2018, Brazil accounted for 10% of global cattle production, 7% of global maize, and 34% of global soybeans (FAOSTAT).

³¹The Brazilian Amazon accounts for 4.1% of the beef world supply (FAO and IBGE) and our efficient land use implies a reduction of 95% in the area devoted to cattle grazing, implying a 4% reduction in world supply. Assuming the supply elasticity across the globe is the same as the one we compute for the Brazilian Amazon (1.43) and demand elasticity of -0.45 (Brester and Wohlgemant, 1993), we find a small world price equilibrium effect of $4.16\% = 4\%/(0.45 + 1.43)$.

Trade. There is growing concern about the extent to which international trade may affect deforestation (Harstad, 2024b), be it through trade agreements (Abman and Lundberg, 2020; Farrokhi et al., 2023; Abman et al., 2024) or international demand for commodities (Harding et al., 2021; Carreira et al., 2024). Although not our main focus, here we exploit the same partial equilibrium setting to study the decrease of trade barriers for Brazilian beef. As an illustrative example, we consider the potential deforestation effects of a trade agreement between the European Union (EU) and Mercosur. We build a partial equilibrium model in which Brazilian beef is bought by the EU and the Rest of the World (ROW), including the domestic market. We show in Appendix A.3 how to approximate the domestic price effect of a change in EU tariff by

$$\frac{dp}{p} \approx s \frac{\epsilon^D}{\epsilon^S - \epsilon^D} dt = -0.06 \frac{0.45}{1.43 + 0.45} dt = -0.014dt, \quad (20)$$

where s is the share of exports to the EU out of the Brazilian beef supply, ϵ^S is the Brazilian beef supply, and ϵ^D is beef demand, assumed equal across EU and the ROW. We use the same numbers for the supply and demand elasticities used in the previous exercise and the share of exports to EU of 6%.³²

We consider the extreme case in which the EU-Mercosur agreement eliminates the 20% EU tariff on Brazilian beef³³ and all non-tariff barriers, also estimated to be about 20% for agricultural commodities (Cadot et al., 2018). Equation (20) then implies that a potential EU-Mercosur trade agreement would increase domestic beef prices by $0.014 \times 0.40 = 0.6\%$. The estimated elasticity of forest cover with respect to cattle prices (-1.66) implies a $0.6 \times 1.66 = 1.00\%$ decrease in forest cover, which amounts to a total additional deforestation of 9,500 sq km (equivalent to one year of deforestation). This forest loss would release 0.46 Gt CO₂ (equivalent to \$23 billion of damage considering the social cost of carbon of \$50 per ton of CO₂). This exercise highlights the importance of conditionality clauses for trade agreements, which can prevent the environmental damages implied by standard free trade agreements (Harstad, 2024a).

³²As in any back-of-the-envelope analysis, the exercise presented here has limitations. First, this is a partial equilibrium model that does not incorporate other sources for beef demand. In reality, the demand for beef faced by Brazilian producers should be more elastic. However, any elasticity value in the inelastic range would produce similar results. Second, this approximates well the effect of marginal tariff changes, holding fixed the share s , which may not be reasonable for all trade agreements.

³³<https://trade.ec.europa.eu/access-to-markets/en/results?product=0201300031&origin=BR&destination=DE>.

7.3 Carbon stock accounting

Forest regeneration. Our baseline model features a direct transition between crop and pasture to the forest state. When calculating carbon emissions, we assumed the aggregate steady-state forest cover holds its full carbon stock potential. However, fields that return to the forest state may take decades to recoup their carbon potential by natural regeneration.³⁴ This will not matter for land use in the carbon tax counterfactual, since we assume the tax is implemented over the potential carbon stock, but it may be important for long-run emissions.

To assess how sensitive our results are to this simplification, we consider an extreme opposite scenario in which a field converted to forest holds zero carbon in the first 30 years.³⁵ Table D.7 shows that in this scenario, the difference between the BAU and the efficient carbon pricing would imply fewer 58 billion tons of CO_2 emitted, compared to 42 billion tons in our baseline. However, the amount of avoided emissions from small values of carbon tax is similar to our baseline. E.g., a \$10/ton carbon tax saves 40 billion tons relative to BAU in our baseline (Table D.3) and 49 billion tons in this extreme exercise. These results suggest that, while our baseline specification underestimates the size of the BAU-efficient carbon gap, a more complete forestry modeling should not be a game-changer in evaluating small policy changes.

A second concern about the model specification is the possibility that agents transitioning from secondary vegetation to other land uses may have significantly different behavior than those transitioning from native vegetation. To alleviate this concern, we estimate our model using a smaller sample that includes only pixels that had been already deforested before 2008, effectively estimating the parameters governing land use decisions in places with secondary vegetation. Column 4 of Tables D.2,D.4, and D.5 show the estimates of the model with this subsample. Table D.6 Panel C shows that, using estimates from the restricted sample, the gap between BAU and the efficient scenarios amounts to 1,408,000 km^2 and 58 billion tons of CO_2 , compared to 1,186,000 km^2 and 42 billion tons of CO_2 in our main specification.

Peatland. In our main specification, we only consider aboveground carbon stock. This ignores the potential relevance of belowground carbon released by deforestation, especially carbon stored in peatlands. We address two concerns related to this point.

First, our current counterfactuals may underestimate the long-run BAU carbon emissions by not considering carbon released from the ground. The main challenge to directly address this point is that estimates of peatland area in South America are very imprecise

³⁴Forest biomass regeneration is faster at the beginning of the regeneration process and slows down over time. After 25 years, it recoups 70% of its original biomass (Houghton et al., 2000).

³⁵We provide details for this exercise in Appendix B.3.

and vary from 100,000 to 900,000 sq. km (Xu et al., 2018), and there are no reliable data on the carbon density of peatlands in the region (Ribeiro et al., 2021). There is also further uncertainty about how much belowground carbon is released by deforestation (Baccini et al., 2012). Given the difficulty of measuring belowground carbon stock, current Brazilian policy instruments, including the Amazon Fund, do not account for belowground carbon emissions and only consider aboveground carbon emissions. Therefore, while our counterfactuals likely underestimate BAU carbon emissions, our counterfactuals are policy-relevant.

Second, peatlands might be a source of unobserved heterogeneity which could affect our estimates. To assess the sensitivity of our estimates to the presence of peatlands, we estimate our model only in a subsample excluding pixels within peatlands using the location of peatlands from the Global Forest Watch. Tables D.4 and D.5 column 5 show that the model estimates are nearly unchanged by the exclusion of peatlands. Panel D in Table D.6 shows that the forest and carbon gaps computed with these estimates are similar to the gaps computed using our main specification. Thus, this exercise suggests that peatlands do not imply considerable uncertainty about model estimates.

7.4 Technical assumptions

Discount rate. As in most applications, we do not estimate the discount factor as it is poorly identified (Rust, 1994). We re-estimated the model and counterfactuals with a discount factor of 0.95. In our application, this sensitivity analysis is particularly relevant since different degrees in property rights imply different eviction risks, which would manifest in the model as heterogeneity in discount rates.³⁶ Most changes to model estimates refer to conversion cost parameters (Table D.5, column 3), which are generally lower than in our baseline. Results for main counterfactuals of interest are reported in Table D.6 Panel B. This exercise suggests a larger carbon gap of 53Gt of CO₂. Qualitatively, the effects of the efficient policy instrument are similar and a \$10 carbon tax would close 92% of the gap in carbon emissions.

Technology. We study the equilibrium choices under technologies currently in use in the Amazon, but farmers in the region could slowly adopt more productive technologies over time. As a robustness check, we estimate an extension of the model where we model the return of agriculture using the most productive technology available in nearby regions in Brazil, the soy-maize double cropping system. Column 2 in Tables D.4 and D.5 shows that,

³⁶An additional complexity arises if the discount rate becomes endogenous to land-use decisions, for instance, if converting forest to pasture increases property claims. We lack the tools and good land tenure data to explore further this mechanism, which remains a topic for future research.

with double cropping, the carbon value that rationalizes land use is R\$2.86/ton per year. Table D.6 Panel A shows that the efficient steady state would prevent 37 billion tons of CO_2 from being released into the atmosphere relative to the BAU steady state.

8 Conclusion

In this paper, we estimate the efficient level of carbon storage in the Brazilian Amazon using an original dynamic discrete choice land-use model. We use the estimated model to compute the long-run carbon emission gap between the optimal forest cover and the one we would have under business-as-usual practices. We estimate this gap amounts to 42 billion tons of CO_2 , with 92% from forest conversion to pasture. These results show cattle ranching will remain a significant driver of deforestation in the Amazon in the long run. We also use the model to quantify the effectiveness and welfare implications of a land-use carbon tax (or PES) based on the potential carbon content of the land and excise taxes on cattle ranching and crops. The carbon tax, by acting directly in the externality, is the first-best policy instrument since it can implement the carbon-efficient land use. We find a very convex response of carbon emissions from deforestation to carbon taxes, such that relatively small carbon taxes can mitigate a substantial part of inefficient emissions. We find that the second-best policy, a 100% tax on cattle ranching, achieves 87% of the welfare gains of a carbon tax.

While the logistics of implementing a carbon tax or PES are not simple, we understand that a practical implementation would require four key elements. First, effective technology to identify deforestation on a large scale. Brazil has demonstrated that it can use technology to enforce environmental compliance (Assunção et al., 2023a). Second, a reliable registry to identify landowners. Although land tenure in the Amazon is complex, Brazil has invested in a national land registry, which can pinpoint the exact boundaries of rural properties and their owners. This land registry has been used to reduce deforestation (Alix-Garcia et al., 2018). Third, a mechanism to either reward landowners for preserving the forest or penalize those who deforest. Brazil’s new instant payment system facilitates direct payments to landowners with smartphone and internet access. Alternatively, the regulatory framework established by the New Forest Code of 2012 provides a basis for enforcing fines. Fourth, data on the potential carbon stock of the land, which is publicly available from different sources. Thus, we understand that Brazil has the main tools needed to implement the policies we study.

As with any research paper, ours has some limitations imposed by model assumptions and the data. Perhaps the most important limitation is that we cannot account for the value of lost biodiversity or other non-carbon externalities associated with deforestation,

such as tipping points. Therefore, the optimal forest gap we estimate should be seen as a lower bound. Nevertheless, we believe the numbers provided in this paper make a sensible contribution by quantifying how the current land use pattern in the Amazon is driving the region very far away from its long-run efficient forest cover, and by informing the policy debate surrounding the mitigation of carbon emissions from land-use change in the Amazon.

References

- Abman, R. and Lundberg, C. (2020). Does Free Trade Increase Deforestation? The Effects of Regional Trade Agreements. *Journal of the Association of Environmental and Resource Economists*, 7(1):35–72.
- Abman, R., Lundberg, C., and Ruta, M. (2024). The Effectiveness of Environmental Provisions in Regional Trade Agreements. *Journal of the European Economic Association*.
- Aguirregabiria, V. and Magesan, A. (2013). Euler Equations for the Estimation of Dynamic Discrete Choice Structural Models. In Choo, E. and Shum, M., editors, *Advances in Econometrics*, volume 31, pages 3–44. Emerald Group Publishing Limited.
- Aguirregabiria, V. and Mira, P. (2007). Sequential Estimation of Dynamic Discrete Games. *Econometrica*, 75(1):1–53.
- Alix-Garcia, J. and Millimet, D. L. (2022). Remotely Incorrect. *Journal of the Association of Environmental and Resource Economists*.
- Alix-Garcia, J., Rausch, L. L., L’Roe, J., Gibbs, H. K., and Munger, J. (2018). Avoided Deforestation Linked to Environmental Registration of Properties in the Brazilian Amazon. *Conservation Letters*, 11(3):e12414.
- Alix-Garcia, J. M., Sims, K. R., and Yañez-Pagans, P. (2015). Only One Tree from Each Seed? Environmental Effectiveness and Poverty Alleviation in Mexico’s Payments for Ecosystem Services Program. *American Economic Journal: Economic Policy*, 7(4):1–40.
- Anderson, T. W. and Hsiao, C. (1981). Estimation of Dynamic Models with Error Components. *Journal of the American Statistical Association*, 76(375):598–606.
- Araujo, R. (2022). When Clouds Go Dry: An Integrated Model of Deforestation, Rainfall, and Agriculture. *Working paper*.
- Araujo, R., Assunção, J., Hirota, M., and Scheinkman, J. A. (2023). Estimating the spatial amplification of damage caused by degradation in the amazon. *Proceedings of the National Academy of Sciences*, 120(46):e2312451120.
- Arellano, M. and Bond, S. (1991). Some Tests of Specification for Panel Data: Monte Carlo Evidence and an Application to Employment Equations. *Review of Economic Studies*, 58(2):277–297.

- Asher, S., Garg, T., and Novosad, P. (2020). The Ecological Impact Of Transportation Infrastructure. *Economic Journal*. ueaa013.
- Assunção, J., Gandour, C., and Rocha, R. (2023a). DETER-ing Deforestation in the Amazon: Environmental Monitoring and Law Enforcement. *American Economic Journal: Applied Economics*, 15(2):125–156.
- Assunção, J., McMillan, R., Murphy, J., and Souza-Rodrigues, E. (2023b). Optimal Environmental Targeting in the Amazon Rainforest. *The Review of Economic Studies*, 90(4):1608–1641.
- Assunção, J., Gandour, C., and Rocha, R. (2015). Deforestation Slowdown in the Brazilian Amazon: Prices or Policies? *Environment and Development Economics*, 20(6):697–722.
- Assunção, J. and Rocha, R. (2019). Getting Greener by Going Black: the Effect of Blacklisting Municipalities on Amazon Deforestation. *Environment and Development Economics*, 24(2):115–137.
- Baccini, A., Goetz, S. J., Walker, W., Laporte, N. T., Sun, M., Sulla-Menashe, D., et al. (2012). Estimated Carbon Dioxide Emissions from Tropical Deforestation Improved by Carbon-Density Maps. *Nature Climate Change*, 2(3):182–185.
- Brester, G. W. and Wohlgemant, M. K. (1993). Correcting for Measurement Error in Food Demand Estimation. *The Review of Economics and Statistics*, 75(2):352–356.
- Burgess, R., Costa, F., and Olken, B. (2019). The Brazilian Amazon’s Double Reversal of Fortune. Technical report.
- Bustos, P., Caprettini, B., and Ponticelli, J. (2016). Agricultural Productivity and Structural Transformation: Evidence from Brazil. *American Economic Review*, 106(6):1320–65.
- Cadot, O., Gourdon, J., and Van Tongeren, F. (2018). Estimating ad valorem equivalents of non-tariff measures: Combining price-based and quantity-based approaches.
- Carreira, I., Costa, F., and Pessoa, J. P. (2024). The deforestation effects of trade and agricultural productivity in brazil. *Journal of Development Economics*, 167:103217.
- Chambers, J. Q., Higuchi, N., Schimel, J. P., Ferreira, L. V., and Melack, J. M. (2000). Decomposition and carbon cycling of dead trees in tropical forests of the central amazon. *Oecologia*, 122:380–388.
- Chimeli, A. B. and Soares, R. R. (2017). The Use of Violence in Illegal Markets: Evidence from Mahogany Trade in the Brazilian Amazon. *American Economic Journal: Applied Economics*, 9(4):30–57.
- Chomitz, K. and Gray, D. A. (1999). *Roads, Lands, Markets, and Deforestation: A Spatial Model of Land Use in Belize*. The World Bank.

- Coad, L., Campbell, A., Miles, L., and Humphries, K. (2008). The Costs and Benefits of Protected Areas for Local Livelihoods: A Review of the Current Literature. *UNEP World Conservation Monitoring Centre, Cambridge, UK*.
- Cochrane, M. A. (2003). Fire science for rainforests. *Nature*, 421(6926):913–919.
- Costinot, A., Donaldson, D., and Smith, C. (2016). Evolving Comparative Advantage and the Impact of Climate Change in Agricultural Markets: Evidence from 1.7 Million Fields Around the World. *Journal of Political Economy*, 124(1):205–248.
- De Azevedo, T. R., Junior, C. C., Junior, A. B., dos Santos Cremer, M., Piatto, M., Tsai, D. S., Barreto, P., Martins, H., et al. (2018). SEEG Initiative Estimates of Brazilian Greenhouse Gas Emissions from 1970 to 2015. *Scientific Data*, 5:180045.
- Dominguez-Iino, T. (2021). Efficiency and Redistribution in Environmental Policy: An Equilibrium Analysis of Agricultural Supply Chains. Technical report, working paper.
- Donaldson, D. (2018). Railroads to Raj. *American Economic Review*, 108(4-5):899–934.
- Donaldson, D. and Hornbeck, R. (2016). Railroads and American Economic Growth: A “Market Access” Approach. *Quarterly Journal of Economics*, 131(2):799–858.
- EPA (2016). Social Cost of Carbon. *Environmental Protection Agency (EPA)*: Washington, DC, USA.
- Farrokhi, F., Kang, E., Pellegrina, H. S., and Sotelo, S. (2023). Deforestation: A global and dynamic perspective. *Cited on*, page 6.
- Fezzi, C. and Bateman, I. J. (2011). Structural Agricultural Land Use Modeling for Spatial Agro-Environmental Policy Analysis. *American Journal of Agricultural Economics*, 93(4):1168–1188.
- Flores, B. M., Montoya, E., Sakschewski, B., Nascimento, N., Staal, A., Betts, R. A., Levis, C., Lapola, D. M., Esquivel-Muelbert, A., Jakovac, C., et al. (2024). Critical transitions in the amazon forest system. *Nature*, 626(7999):555–564.
- Franklin Jr, S. L. and Pindyck, R. S. (2018). Tropical Forests, Tipping Points, and the Social Cost of Deforestation. *Ecological Economics*, 153:161–171.
- GAEZ, F. (2012). Global Agro-ecological Zones (GAEZ v3.0). *IIASA, Laxenburg, Austria and FAO, Rome, Italy*.
- Gatti, L. V., Basso, L. S., Miller, J. B., Gloor, M., Gatti Domingues, L., Cassol, H. L., Tejada, G., Aragão, L. E., Nobre, C., Peters, W., et al. (2021). Amazonia as a carbon source linked to deforestation and climate change. *Nature*, 595(7867):388–393.
- Hansen, M. C., Potapov, P. V., Moore, R., Hancher, M., Turubanova, S., Tyukavina, A., Thau, D., Stehman, S., Goetz, S., Loveland, T., et al. (2013). High-Resolution Global Maps of 21st-Century Forest Cover Change (v1.6). *Science*, 342(6160):50–853.

- Harding, T., Herzberg, J., and Kuralbayeva, K. (2021). Commodity Prices and Robust Environmental Regulation: Evidence from Deforestation in Brazil. *Journal of Environmental Economics and Management*, 108:102452.
- Harstad, B. (2024a). Contingent Trade Agreements. Technical report, National Bureau of Economic Research.
- Harstad, B. (2024b). Trade and Trees. *American Economic Review: Insights (Forthcoming)*.
- Heilmayr, R., Echeverría, C., and Lambin, E. F. (2020). Impacts of Chilean Forest Subsidies on Forest Cover, Carbon and Biodiversity. *Nature Sustainability*, 3(9):701–709.
- Hornbeck, R. (2010). Barbed Wire: Property Rights and Agricultural Development. *Quarterly Journal of Economics*, 125(2):767–810.
- Hotz, V. J. and Miller, R. A. (1993). Conditional Choice Probabilities and the Estimation of Dynamic Models. *Review of Economic Studies*, 60(3):497–529.
- Houghton, R., Skole, D., Nobre, C. A., Hackler, J., Lawrence, K., and Chomentowski, W. H. (2000). Annual Fluxes of Carbon from Deforestation and Regrowth in the Brazilian Amazon. *Nature*, 403(6767):301–304.
- Hsiao, A. (2021). Coordination and Commitment in International Climate Action: Evidence from Palm Oil. Technical report, working paper.
- IPCC (2003). Good Practice Guidance for Land Use, Land-Use Change and Forestry. Penman, J., Gytarsky, M., Hiraishi, T., et al.
- IPCC (2019). 2019 Refinement to the 2006 IPCC Guidelines for National Greenhouse Gas Inventories. Volume 4 Agriculture, Forestry and Other Land Use. Calvo Buendia, E., Tanabe, K., Kranjc, A., Baasansuren, J., et al. (eds). Published: IPCC, Switzerland.
- Jayachandran, S., De Laat, J., Lambin, E. F., Stanton, C. Y., Audy, R., and Thomas, N. E. (2017). Cash for Carbon: A Randomized Trial of Payments for Ecosystem Services to Reduce Deforestation. *Science*, 357(6348):267–273.
- Kalouptsidi, M., Scott, P. T., and Souza-Rodrigues, E. (2021). Linear IV Regression Estimators for Structural Dynamic Discrete Choice Models. *Journal of Econometrics*, 222(1):778–804.
- Liang, J., Gamarra, J. G., Picard, N., Zhou, M., Pijanowski, B., Jacobs, D. F., Reich, P. B., Crowther, T. W., Nabuurs, G.-J., De-Miguel, S., et al. (2022). Co-limitation towards lower latitudes shapes global forest diversity gradients. *Nature ecology & evolution*, 6(10):1423–1437.
- Lubowski, R. N., Plantinga, A. J., and Stavins, R. N. (2006). Land-use Change and Carbon Sinks: Econometric Estimation of the Carbon Sequestration Supply Function. *Journal of Environmental Economics and Management*, 51(2):135–152.

Malhi, Y., Roberts, J. T., Betts, R. A., Killeen, T. J., Li, W., and Nobre, C. A. (2008). Climate Change, Deforestation, and the Fate of the Amazon. *Science*, 319(5860):169–172.

MapBiomas, P. (2019). Collection 4.0.

Matricardi, E. A. T., Skole, D. L., Costa, O. B., Pedlowski, M. A., Samek, J. H., and Miguel, E. P. (2020). Long-term Forest Degradation Surpasses Deforestation in the Brazilian Amazon. *Science*, 369(6509):1378–1382.

McKay, A., I, D., Staal, A., et al. (2022). Exceeding 1.5 °C global warming could trigger multiple climate tipping points. *Science*, 377(6611):eabn7950.

MCTI (2020). Quarta Comunicação Nacional do Brasil à Convenção-Quadro das Nações Unidas sobre Mudança do Clima.

Nepstad, D., McGrath, D., Stickler, C., Alencar, A., Azevedo, A., et al. (2014). Slowing Amazon Deforestation Through Public Policy and Interventions in Beef and Soy Supply Chains. *Science*, 344(6188):1118–1123.

Nobre, C. A., Sellers, P. J., and Shukla, J. (1991). Amazonian deforestation and regional climate change. *Journal of Climate*, 4(10):957–988.

Nolte, C., Agrawal, A., Silvius, K. M., and Soares-Filho, B. S. (2013). Governance Regime and Location Influence Avoided Deforestation Success of Protected Areas in the Brazilian Amazon. *Proceedings of the National Academy of Sciences*, 110(13):4956–4961.

Nordhaus, W. (2014). Estimates of the Social Cost of Carbon: Concepts and Results from the DICE-2013R Model and Alternative Approaches. *Journal of the Association of Environmental and Resource Economists*, 1(1/2):273–312.

Pellegrina, H. (2020). Trade, Productivity, and the Spatial Organization of Agriculture: Evidence from Brazil. Technical report, working paper.

Pendrill, F., Gardner, T. A., Meyfroidt, P., Persson, U. M., Adams, J., Azevedo, T., et al. (2022). Disentangling the Numbers Behind Agriculture-Driven Tropical Deforestation. *Science*, 377(6611):eabm9267.

Ribeiro, K., Pacheco, F. S., Ferreira, J. W., de Sousa-Neto, E. R., Hastie, A., Krieger Filho, G. C., Alvalá, P. C., et al. (2021). Tropical peatlands and their contribution to the global carbon cycle and climate change. *Global Change Biology*, 27(3):489–505.

Rogelj, J., Shindell, D., Jiang, K., Fifita, S., Forster, P., Ginzburg, V., et al. (2018). Mitigation Pathways Compatible with 1.5°C in the Context of Sustainable Development. In *Global Warming of 1.5°C. An IPCC Special Report on the impacts of global warming of 1.5°C above pre-industrial levels and related global greenhouse gas emission pathways, in the context of strengthening the global response to the threat of climate change, sustainable development, and efforts to eradicate poverty*. Intergovernmental Panel on Climate Change (IPCC).

- Rosen, S., Murphy, K. M., and Scheinkman, J. A. (1994). Cattle Cycles. *Journal of Political Economy*, 102(3):468–492.
- Rust, J. (1994). Chapter 51 Structural Estimation of Markov Decision Processes. In *Handbook of Econometrics*, volume 4, pages 3081–3143. Elsevier.
- Sampaio, G., Nobre, C., Costa, M. H., Satyamurty, P., Soares-Filho, B. S., and Cardoso, M. (2007). Regional climate change over eastern amazonia caused by pasture and soybean cropland expansion. *Geophysical Research Letters*, 34(17).
- Sant'Anna, M. (2024). How Green Is Sugarcane Ethanol? *The Review of Economics and Statistics*, 106(1):202–216.
- Scott, P. (2013). Dynamic Discrete Choice Estimation of Agricultural Land Use. Technical report.
- Soares-Filho, B., Moutinho, P., Nepstad, D., Anderson, A., Rodrigues, H., Garcia, R., et al. (2010). Role of Brazilian Amazon Protected Areas in Climate Change Mitigation. *Proceedings of the National Academy of Sciences*, 107(24):10821–10826.
- Soares-Filho, B. S., Nepstad, D. C., Curran, L. M., Cerqueira, G. C., et al. (2006). Modelling Conservation in the Amazon Basin. *Nature*, 440(7083):520–523.
- Souza-Rodrigues, E. (2019). Deforestation in the Amazon: A Unified Framework for Estimation and Policy Analysis. *Review of Economic Studies*, 86(6):2713–2744.
- Spracklen, D. V., Arnold, S. R., and Taylor, C. (2012). Observations of Increased Tropical Rainfall Preceded by Air Passage Over Forests. *Nature*, 489(7415):282–285.
- Staal, A., Tuinenburg, O. A., Bosmans, J. H., Holmgren, M., van Nes, E. H., Scheffer, M., Zemp, D. C., and Dekker, S. C. (2018). Forest-rainfall cascades buffer against drought across the amazon. *Nature Climate Change*, 8(6):539–543.
- Torchiana, A. L., Rosenbaum, T., Scott, P. T., and Souza-Rodrigues, E. (2022). Improving Estimates of Transitions from Satellite Data: A Hidden Markov Model Approach. *Review of Economics and Statistics*.
- Wong, P. Y., Harding, T., Kuralbayeva, K., Anderson, L. O., and Pessoa, A. M. (2019). Pay for Performance and Deforestation: Evidence from Brazil. Technical report.
- Xu, J., Morris, P. J., Liu, J., and Holden, J. (2018). PEATMAP: Refining estimates of global peatland distribution based on a meta-analysis. *CATENA*, 160:134–140.
- Zarin, D. J., Harris, N. L., Baccini, A., et al. (2016). Can Carbon Emissions from Tropical Deforestation Drop by 50% in 5 Years? *Global Change Biology*, 22(4):1336–1347.

Appendix (for online publication)

- **Appendix A** presents additional model derivations.
 - **Appendix A.1** presents details on the derivation of the regression equation.
 - **Appendix A.2** derives the equation that serves as the basis of our welfare analysis.
 - **Appendix A.3** presents the simple partial equilibrium model that helps us illustrate the effects of a decrease in tariffs on Brazilian beef.
- **Appendix B** describes in details how we compute the transportation costs, the conditional choice probabilities, and the counterfactual without regeneration discussed in section 7.3.
- **Appendix C** provides additional evidence of forest regeneration in our setting.
- **Appendix D** shows the supporting figures and tables.

A Model appendix

A.1 Regression equation derivation details

Here we provide more details on the derivation of the regression equation. The derivation below largely follows the steps in Scott (2013). From (3) and (6), we have:

$$\begin{aligned} \Phi_{jk}(w_{mt}; \varphi) + r_j(w_{mt}; \alpha) - \Phi_{j'k}(w_{mt}; \varphi) - r_{j'}(w_{mt}; \alpha) - \log \left(\frac{p(j|k, w_{mt})}{p(j'|k, w_{mt})} \right) = \\ \rho E [\bar{V}(j', w_{m,t+1})|w_{mt}] - \rho E [\bar{V}(j, w_{m,t+1})|w_{mt}], \text{ for } k, j, j' \in J. \end{aligned} \quad (\text{A.1})$$

Let $\eta_j^V(w_{mt}) := \rho(E[\bar{V}(j, w_{m,t+1})|w_{mt}] - \bar{V}(j, w_{m,t+1}))$ denote the expectation error in continuation values. We can re-write (A.1) as

$$\begin{aligned} \Phi_{jk}(w_{mt}; \varphi) + r_j(w_{mt}; \alpha) - \Phi_{j'k}(w_{mt}; \varphi) - r_{j'}(w_{mt}; \alpha) - \log \left(\frac{p(j|k, w_{mt})}{p(j'|k, w_{mt})} \right) = \\ \rho(\bar{V}(j', w_{m,t+1}) - \bar{V}(j, w_{m,t+1})) + \eta_{j'}^V(w_{mt}) - \eta_j^V(w_{mt}), \text{ for } k, j, j' \in J. \end{aligned} \quad (\text{A.2})$$

Another implication of the logit errors assumption is that $\bar{V}(j', w_{mt})$ has a convenient expression:

$$\bar{V}(k, w_{mt}) = \log \left(\sum_{j \in J} \exp(v(j, k, w_{mt})) \right) + \gamma, \text{ for all } k \in J, \quad (\text{A.3})$$

where γ is the Euler's gamma. From (5) and (A.3), for all $k \in J$, we can write

$$\bar{V}(k, w_{mt}) = v(\ell, k, w_{mt}) - \log(p(\ell|k, w_{mt})) + \gamma, \text{ for all } \ell \in J. \quad (\text{A.4})$$

We use the representation in (A.4) to cancel common continuation terms in the difference $\bar{V}(j', w_{m,t+1}) - \bar{V}(j, w_{m,t+1})$ in (A.2). Replacing (A.4) in (A.2), we have

$$\begin{aligned} \Phi_{jk}(w_{mt}; \varphi) + r_j(w_{mt}; \alpha) - \Phi_{j'k}(w_{mt}; \varphi) - r_{j'}(w_{mt}; \alpha) - \log \left(\frac{p(j|k, w_{mt})}{p(j'|k, w_{mt})} \right) = \\ \rho(v(\ell, j', w_{m,t+1}) - v(\ell, j, w_{m,t+1})) - \rho \log \left(\frac{p(\ell|j', w_{m,t+1})}{p(\ell|j, w_{m,t+1})} \right) + \\ \eta_{j'}^V(w_{mt}) - \eta_j^V(w_{mt}), \text{ for } \ell, k, j, j' \in J. \end{aligned} \quad (\text{A.5})$$

From the definition of $v(\cdot)$, $v(\ell, j', w_{m,t+1}) - v(\ell, j, w_{m,t+1}) = \Phi_{\ell j'}(w_{m,t+1}; \varphi) - \Phi_{\ell j}(w_{m,t+1}; \varphi)$.

That is, all continuation terms cancel out and we can simplify further (A.2):

$$\begin{aligned} \Phi_{jk}(w_{mt}; \varphi) + r_j(w_{mt}; \alpha) - \Phi_{j'k}(w_{mt}; \varphi) - r_{j'}(w_{mt}; \alpha) - \log \left(\frac{p(j|k, w_{mt})}{p(j'|k, w_{mt})} \right) = \\ \rho(\Phi_{\ell j'}(w_{m,t+1}; \varphi) - \Phi_{\ell j}(w_{m,t+1}; \varphi)) - \rho \log \left(\frac{p(\ell|j', w_{m,t+1})}{p(\ell|j, w_{m,t+1})} \right) + \\ \eta_{j'}^V(w_{mt}) - \eta_j^V(w_{mt}), \text{ for } \ell, k, j, j' \in J. \quad (\text{A.6}) \end{aligned}$$

Using assumption 3, for $\ell = j$ and $j' = k$, we can re-write (A.6) as

$$\begin{aligned} \log \left(\frac{p(j|k, w_{mt})}{p(k|k, w_{mt})} \right) - \rho \log \left(\frac{p(j|k, w_{m,t+1})}{p(j|j, w_{m,t+1})} \right) = \Phi_{jk}(w_{mt}; \varphi) - \rho \Phi_{jk}(w_{m,t+1}; \varphi) + \\ r_j(w_{mt}) - r_k(w_{mt}) + \eta_j^V(w_{mt}) - \eta_k^V(w_{mt}), \text{ for } j, k \in J. \quad (\text{A.7}) \end{aligned}$$

A.2 Social welfare from policies

When computing social welfare under different policies, one should account for the welfare implications from all choice distortions the policy implies. Here, we establish a general approach to compute welfare from policies under our dynamic setup used in counterfactual exercises in Section 6.5. Suppose we want to evaluate the welfare under a generic policy τ that modifies the private flow return $r_j^\tau(w_m; \alpha)$. For instance, an *ad-valorem* cattle tax would imply a reduction in the private flow return for cattle ranching:

$$r_j^\tau(w_m; \alpha) = \begin{cases} (1 - \tau)r_j(w_m; \alpha) & \text{for } j = \text{pasture}, \\ r_j(w_m; \alpha) & \text{for } j = \text{forest, crop}. \end{cases}$$

The private value function for the farmer's problem (equation 17) is modified by this policy:

$$\bar{V}^\tau(k, w_m) = \log \left(\sum_{j \in J} \exp(\Phi_{j,k}(w_m; \varphi) + r_j^\tau(w_m; \alpha) + \rho \bar{V}^\tau(j, w_m)) \right) + \gamma, \quad (\text{A.8})$$

where γ is the Euler constant. The associated conditional choice probabilities to the farmer's problem are:

$$p^\tau(j|k, w_m) = \frac{\exp(v^\tau(j, k, w_m))}{\sum_{j' \in J} \exp(v^\tau(j', k, w_m))}, \text{ for } k, j \in J, \quad (\text{A.9})$$

where $v^\tau(j, k, w_m) = \Phi_{j,k}(w_m; \varphi) + r_j^\tau(w_m; \alpha) + \rho \bar{V}^\tau(j, w_m)$.

In contrast, define $r_j^s(w_m; \alpha)$ as the social flow return, which in our application should

include the social benefit of carbon of holding forested areas, that is,

$$r_j^s(w_m; \alpha) = \begin{cases} r_j(w_m; \alpha) + s \cdot h_m, & \text{for } j = \text{forest}, \\ r_j(w_m; \alpha), & \text{for } j = \text{crop, pasture}. \end{cases}$$

where s is the flow social value of carbon not directly internalized by the agents. In the applications we consider, the social flow return is not directly affected by policies, which involve only direct transfers of resources between the government and private agents. For example, in the case of cattle taxes, the tax revenue returns directly to society. Policies affect social welfare by changing land-use choices and, therefore, emissions. We can write the social value function under a policy τ as:

$$\tilde{W}^\tau(k, w_m) = \sum_{j \in J} p^\tau(j|k, w_m) \left(\Phi_{j,k}(w_m; \varphi) + r_j^s(w_m; \alpha) + \rho \tilde{W}^\tau(j, w_m) \right), \quad (\text{A.10})$$

where the CCP's $p^\tau(j|k, w_m)$ are determined by the private problem (A.9). The social welfare of a policy τ in location m is computed integrating (A.10) for all choices:

$$\tilde{W}^\tau(w_m) = \sum_{j \in J} \tilde{W}^\tau(j, w_m) \bar{p}^\tau(j, w_m), \quad (\text{A.11})$$

where $\bar{p}^\tau(j, w_m)$ is the steady-state probability of land-use $j \in J$. Finally, the total social welfare of policy τ is then computed summing for all locations

$$\tilde{W}^\tau = \sum_m \tilde{W}^\tau(w_m).$$

Proposition 1 below establishes a convenient way of expressing the social welfare implied by policy τ in location m as the sum of the private value function – which we already calculate for other counterfactual analyses – and the present value of steady-state flow differences between social and private flow returns.

Proposition 1 *We can express the social value function as*

$$\tilde{W}^\tau(w_m) = \bar{V}^\tau(w_m) + \frac{1}{1 - \rho} \sum_{j \in J} \bar{p}^\tau(j, w_m) (r_j^s(w_m; \alpha) - r_j^\tau(w_m; \alpha)), \quad (\text{A.12})$$

where $\bar{V}^\tau(w_m) = \sum_{j \in J} \bar{V}^\tau(j, w_m) \bar{p}^\tau(j, w_m)$ is the private value function after integrating for steady-state land uses.

PROOF. The proof is direct. We begin integrating the social welfare expression (A.10) using

the steady-state invariant land use probabilities:

$$\sum_{k \in J} \bar{p}^\tau(k, w_m) \tilde{W}^\tau(k, w_m) = \sum_{k \in J} \sum_{j \in J} p^\tau(j|k, w_m) \bar{p}^\tau(k, w_m) \left(\Phi_{j,k}(w_m; \varphi) + r_j^s(w_m; \alpha) + \rho \tilde{W}^\tau(j, w_m) \right),$$

which yields the integrated social welfare in (A.12). We can rewrite the expression above as:

$$\begin{aligned} \tilde{W}^\tau(w_m) &= \sum_{k \in J} \sum_{j \in J} p^\tau(j|k, w_m) \bar{p}^\tau(k, w_m) \Phi_{j,k}(w_m; \varphi) + \\ &\quad \sum_{k \in J} \sum_{j \in J} p^\tau(j|k, w_m) \bar{p}^\tau(k, w_m) \left(r_j^s(w_m; \alpha) + \rho \tilde{W}^\tau(j, w_m) \right). \end{aligned}$$

Now we exchange the order of the sum in the last term and note that since $\bar{p}^\tau(\cdot, w_m)$ are the invariant choice probabilities, $\sum_{k \in J} p^\tau(j|k, w_m) \bar{p}^\tau(k, w_m) = \bar{p}^\tau(j, w_m)$:

$$\begin{aligned} \tilde{W}^\tau(w_m) &= \sum_{k \in J} \sum_{j \in J} p^\tau(j|k, w_m) \bar{p}^\tau(k, w_m) \Phi_{j,k}(w_m; \varphi) + \\ &\quad \sum_{j \in J} \left(r_j^s(w_m; \alpha) + \rho \tilde{W}^\tau(j, w_m) \right) \underbrace{\sum_{k \in J} p^\tau(j|k, w_m) \bar{p}^\tau(k, w_m)}_{=\bar{p}^\tau(j, w_m)}. \end{aligned}$$

Next, note that continuation values just aggregate to the steady-state value function:

$$\begin{aligned} \tilde{W}^\tau(w_m) &= \sum_{k \in J} \sum_{j \in J} p^\tau(j|k, w_m) \bar{p}^\tau(k, w_m) \Phi_{j,k}(w_m; \varphi) + \\ &\quad \sum_{j \in J} \bar{p}^\tau(j, w_m) r_j^s(w_m; \alpha) + \rho \underbrace{\sum_{j \in J} \bar{p}^\tau(j, w_m) \tilde{W}^\tau(j, w_m)}_{=\tilde{W}^\tau(w_m)}. \end{aligned}$$

Therefore,

$$\tilde{W}^\tau(w_m) = \frac{1}{1 - \rho} \sum_{k \in J} \sum_{j \in J} p^\tau(j|k, w_m) \bar{p}^\tau(k, w_m) \Phi_{j,k}(w_m; \varphi) + \frac{1}{1 - \rho} \sum_{j \in J} \bar{p}^\tau(j, w_m) r_j^s(w_m; \alpha).$$

As expressed, note that the only difference between the social value function and the farmers' value function is at the flow profits:

$$\bar{W}^\tau(w_m) = \frac{1}{1 - \rho} \sum_{k \in J} \sum_{j \in J} p^\tau(j|k, w_m) \bar{p}^\tau(k, w_m) \Phi_{j,k}(w_m; \varphi) + \frac{1}{1 - \rho} \sum_{j \in J} \bar{p}^\tau(j, w_m) r_j^\tau(w_m; \alpha).$$

Therefore we can express the social value function as

$$\tilde{W}^\tau(w_m) = \bar{V}^\tau(w_m) + \frac{1}{1-\rho} \sum_{j \in J} \bar{p}^\tau(j, w_m) (r_j^s(w_m; \alpha) - r_j^\tau(w_m; \alpha)). \quad (\text{A.13})$$

■

Note again that $r_j^s(w_m; \alpha)$ includes the social carbon value and $r_j^\tau(w_m; \alpha)$ would include tax payments in the case of tax-based policies. For instance, in the case of a cattle tax, the difference in the RHS of (A.12) is

$$r_j^s(w_m; \alpha) - r_j^\tau(w_m; \alpha) = \begin{cases} s \cdot h_m, & \text{if } j = \text{forest}, \\ \tau r_j(w_m; \alpha), & \text{if } j = \text{pasture}, \\ 0, & \text{if } j = \text{crop}. \end{cases}$$

Therefore, in the case of a cattle tax, we can write the social value function as

$$\tilde{W}^\tau(w_m) = \bar{V}^\tau(w_m) + \frac{1}{1-\rho} \bar{p}^\tau(j, w_m) \tau r_j(w_m; \alpha) + \frac{s}{1-\rho} \bar{p}^\tau(\text{forest}, w_m) h_m, \text{ for } j = \text{pasture}. \quad (\text{A.14})$$

The last term is the present value of expected long-run carbon stock.

We can also write the social value function as a function of expected carbon emissions by subtracting from the social value function the present value of the carbon stock in 2000, $s \cdot h_m / (1 - \rho)$. That is, we can define the social value function as

$$W^\tau(w_m) := \tilde{W}^\tau(w_m) - \frac{s \cdot h_m}{1 - \rho},$$

or, substituting from equation (A.14):

$$W^\tau(w_m) = \bar{V}^\tau(w_m) + \frac{1}{1-\rho} \bar{p}^\tau(j, w_m) \tau r_j(w_m; \alpha) - \frac{s}{1-\rho} (1 - \bar{p}^\tau(\text{forest}, w_m)) h_m, \text{ for } j = \text{pasture},$$

where now the last term represents the present value of expected carbon emissions in the long run. Now note that $s / (1 - \rho) =: SCC$ is the present value social cost of carbon emissions not already internalized by private agents.

This allows us to finally decompose the social value function as:

$$W^\tau(w_m) = \bar{V}^\tau(w_m) + \frac{1}{1-\rho} ETAX_m - SCC \times E\Delta CO2_m, \quad (\text{A.15})$$

where $E\Delta CO2_m$ and $ETAX_m$ are, respectively, the expected steady-state carbon emission

relative to carbon stock in 2000 and the expected tax revenue from the cattle tax.

A.3 Partial equilibrium model for Brazilian beef

In this section, we derive the partial equilibrium implications of decreases in tariffs for Brazilian beef by the European Union (EU) discussed in Section 7.2. Let $S(p)$ be the supply of Brazilian beef, where p is the domestic price. EU demand for Brazilian beef is given by $D_{EU}(p\tau)$, where τ is one plus the import tariff applied to Brazilian beef t . The Rest of the World (ROW), including Brazilian domestic demand, is given by $D_X(p)$. Equilibrium in the market for Brazilian beef holds if

$$S(p) = D_{EU}(p\tau) + D_X(p). \quad (\text{A.16})$$

To find the partial equilibrium effects of tariff changes on domestic beef prices, we total differentiate A.16:

$$S'(p)dp = D'_{EU}(p\tau)\tau dp + D'_{EU}(p\tau)p d\tau + D'_X(p)dp$$

Passing to elasticities, the domestic price effect is

$$\frac{dp}{p} = \frac{s \cdot \epsilon_{EU}^D}{\epsilon^S - s \cdot \epsilon_{EU}^D - (1-s)\epsilon_X^D} \frac{d\tau}{\tau},$$

where $s = \frac{D_{EU}(p\tau)}{S(p)}$ is the share of EU imports in Brazilian supply, ϵ_{EU}^D is the EU demand elasticity for Brazilian beef, ϵ_X^D is demand elasticity for the ROW, and ϵ^S is the supply elasticity. Since $\tau = 1 + t$, where t is the tariff, $\frac{d\tau}{\tau} = d\log(\tau) \approx dt$.

So finally,

$$\frac{dp}{p} \approx \frac{s \cdot \epsilon_{EU}^D}{\epsilon^S - s\epsilon_{EU}^D - (1-s)\epsilon_X^D} dt.$$

If we assume that $\epsilon_{EU}^D = \epsilon_X^D =: \epsilon^D$,

$$\frac{dp}{p} \approx s \frac{\epsilon^D}{\epsilon^S - \epsilon^D} dt.$$

We now discuss some of the numbers used in our simple partial equilibrium model. We set $s = 0.06$, which is the share of exports to the EU out of the Brazilian beef supply. Our best guess for the Brazilian beef supply elasticity is our model estimate for the pasture price elasticity, that is, $\epsilon^S = 1.43$. We set beef demand elasticity for EU and the ROW to -0.45

estimated in Brester and Wohlgemant (1993). These numbers imply that the percentage domestic beef price change from a change in EU tariffs is

$$\frac{dp}{p} \approx -0.06 \frac{0.45}{1.43 + 0.45} dt = -0.014dt.$$

B Technical details

B.1 Transportation Costs

We build the cost of transporting agriculture products from each pixel to the nearest export port through several steps and data sources, which we detail in this section.

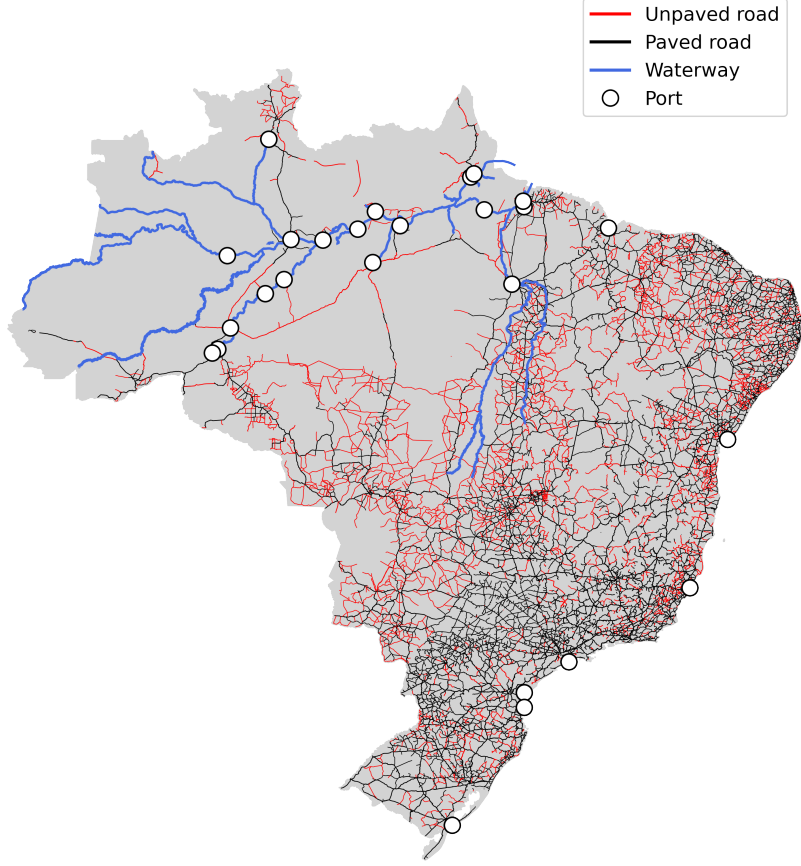
Data on road networks and freight costs. First, we collect georeferenced data on federal and states roads from the National Bureau of Infrastructure DNIT.³⁷ We see there has been little to no development of new roads in Brazil, especially in the Amazon region, over the ten years of analysis. Thus, we assume a stable transportation infrastructure when computing transportation costs. The dataset informs whether each road is paved or unpaved, as shown in Figure B.1. We convert this road network to a raster of the entire Brazilian territory that contains our 1 kilometer grid of locations and assign for each type of terrain a value that represents the cost to traverse that pixel. We allow for four different types of terrain: paved road, unpaved road, land without road, land inside protected areas without road.

Transportation cost by land. The second step is to estimate the cost of transporting agricultural commodities on each type of pixel. We estimate this cost of traversing each type of pixel based on the internal freight costs collected by the Group of Research and Extension in Agroindustrial Logistics of the College of Agriculture Luiz de Queiroz (ESALQ). This data contains the transportation costs per ton of each product (maize and soy) between multiple municipalities for the years 2008-2013. We keep only pairs of origin/destination municipalities that connect at least one of the states of the Legal Amazon – Figure B.2 plots all origin/destination pairs we use.

We estimate the transportation cost of each type of pixel using a non-linear least squares (NLSS) as Donaldson (2018). To do so, we first set up a grid of possible values for the costs of traversing each type of road, which we denote θ . For each θ , we apply Dijkstra's shortest path algorithm to generate an estimated (non-monetary) cost of transiting products from origin m to destination n for all origin/destination pairs (m, n) in the ESALQ's data. Let $TransitCost_{m,n}(\theta)$ be the cost calculated in this process. Note that this measure has no monetary interpretation. We use ESALQ's freight cost to estimate the monetary transportation cost based on θ . For each θ , we regress the freight cost for each product and

³⁷Visited on 11/18/2018, <http://www.dnit.gov.br/mapas-multimodais/shapefiles>.

Figure B.1: Federal and state roads networks



This map shows the state and federal road, waterways, and ports network we use to compute transportation costs. Black lines show paved roads and red lines show unpaved roads. The waterways are shown in blue with the ports in white circles. The ports on the coast are the ones which we consider to have direct access to international market

origin/destination pairs (m, n) on our non-monetary transit cost:

$$FreightCost_{m,n,c} = \beta_{0,c} + \beta_{1,c}TransitCost_{m,n}(\theta) + \epsilon_{m,n,c}, \quad (\text{B.1})$$

where $FreightCost_{m,n,c}$ is the monetized freight cost of transportation of one ton of product c between municipalities i and j from the ESALQ's dataset. The least squares objective function will be naturally linear in $\beta_{0,c}$ and $\beta_{1,c}$, but non-linear in θ due to the Dijkstra's algorithm. We choose the set of parameters θ that delivers the highest average R-squared.

The estimates of the best fit model is described in Table B.1. This gives us the relative costs of transporting each product by land in the whole region. This model sets the cost of

Figure B.2: Pairs of origin/destination freight costs from ESALQ



Each black line in the map represents an origin/destination pair in the ESALQ freight costs dataset.

traveling over pixels with paved roads equal to 1, unpaved road equal to 2, pixels with no state or federal roads equal to 5, and pixels without roads inside protected areas equal to 10. These values, especially for protected areas, seem low when compared with calibrated values from the literature (see, e.g., Souza-Rodrigues, 2019). Nonetheless, increasing the cost of travelling over pixels inside protected areas do not make much difference for the estimation because our estimated parameters are already high enough that agents avoid travelling by these pixels.

To clarify some technical aspects, the underlying data structure to compute those costs is a graph, where each pixel is a node and possible connections between pixels are edges. To keep using the raster analogy, each pixel is connected with its 8 neighbors, provided they are inside Brazil. To visit a pixel, the agent must pay the value of that pixel. To increase the precision of our algorithm, movement in the diagonal is multiplied by $\sqrt{2}$, to account for the fact that pixels in the diagonal are farther away than the others.

Transportation cost by water. Third, we calculate the transportation cost by waterways, a commonly used transportation mode in the Amazon. Differently from roads, we

Table B.1: Estimates to monetize transportation cost

	Soybeans (1)	Maize (2)
Coefficient (β_1)	0.07 (0.01)	0.07 (0.01)
Constant (β_0)	5.32 (1.34)	7.79 (1.41)
R^2	0.84	0.88
N. obs	1,200	972

This table presents the estimates of the non-linear least squares regressions from equation (B.1).

cannot quantify the transportation costs between all origin/destination pairs. Instead, we model waterway transportation as an expressway to reach international markets. To do so, we collected georeferenced data on all Brazilian ports and waterways from the Ministry of Transportation. We differentiate between two types of ports: (i) final ports in which goods can be directly shipped to the international market, those with easy access to the sea; and (ii) loading ports, used as entrance to the waterways. We set the cost to traverse a pixel with waterway equal to half the cost to traverse a paved road. Figure B.1 shows the location of the waterways and ports.

Minimum shipping costs. In the last step, equipped with the transit costs by roads and by waterways, we compute the minimum cost to ship products from every location in our sample to the nearest final port, using Dijkstra's algorithm. We transform this transit cost to a monetary value using the predicted values from equation (B.1). We end up with a monetary cost to transport each product from each location to an international port.

Going back to the graph data structure, a waterway node can only have an edge with another node if it is also a waterway or a port. This is how we guarantee that an agent has to go through a port to access the waterway. To keep the raster analogy, our transportation network can be seen as a three dimensional raster: one layer representing land and roads; a second layer representing waterways. Once in the waterway layer, the agent can only move on waterways. To go from the roads' layer to the waterways' layer the agent must access a port pixel.

B.2 Conditional Choice Probabilities

In this section we describe in more detail the computation of the conditional probabilities that make the left hand side of our main regressions. Figure B.3 shows each step of the procedure.

We start with our land use data ((a) and (b)) for two consecutive years – say 2008 and 2009. In this data we flag pixels that are out of our sample – other countries, oceans, protected areas, pixels deforested before 2000, pixels classified as urban areas or water. In step (c), for a possible transition – say forest to crop – we create a new image where we assign 1 to the pixel that made this transition and zero otherwise. Notice that we keep flagged the pixels out of our sample. In step (d), we reduce the resolution of the image – from 30 meters to 1 km in the paper, but for illustration purposes here we reduce from 4 pixels to 1 – by taking the average values. This step will still result in an image with many zeros.

In step (e) and (f), we select a pixel in our sample and apply the Gaussian filter. The Gaussian filter will take an average of the pixels around the selected pixel (flagged with a red square in (e)), assigning less weight to pixels that are farther away. These weights are determined by a Gaussian distribution with zero mean and standard deviation of 150 km. Analytically, the distribution should touch all pixels, since the Gaussian distribution has unbounded support. But, computationally the values are capped at 3 standard deviations. In this step, we exclude pixels out of our sample. In other words, we compute a normalized convolution.

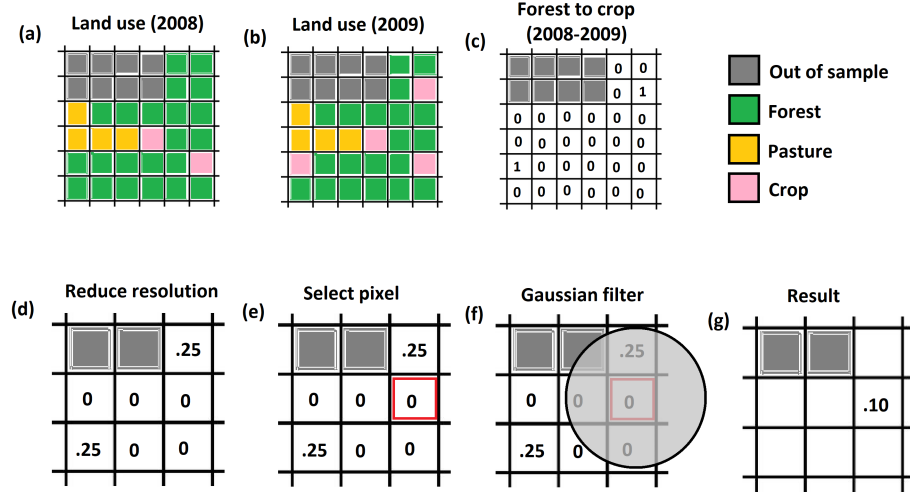
In (g) we show the computed conditional probability for the selected pixel. Finally, we repeat the steps (e) and (f) for every pixel in our sample, including the non-zero ones. The result of each pixel will fill the Result image in (g). We then repeat all steps for every pair of consecutive years and every possible transition.

B.3 Carbon Accounting with Forest Regeneration

As described in Section 6, to compute the counterfactual land use we begin by computing the transition matrix for each pixel. We then compute the invariant distribution of land use for each pixel. Let Table B.2 represent the transition matrix of a pixel in a given scenario. In this matrix, the value (row,column) shows the conditional probability of the pixel transitioning from land use row to land use column.

To compute the invariant distribution of each pixel in the scenario with forest regeneration we modify the above transition matrix as depicted in Table B.3. In this scenario we shut down the channel of transition from crop and pasture directly to forest. Once deforested, a

Figure B.3: Computing the conditional probability



This figure shows the steps we take to compute the conditional probability of land use transition. (a) and (b) show land use data, where each color corresponds to a possible use (forest, pasture, crop and out of sample); (c) illustrates the image that flags pixels that made the transition from forest to crop between 2008 and 2009 as 1. From (c) to (d) the resolution of the image is diminished by a factor of 4. The resulted image is an average of the nearby pixels, ignoring the pixels out of sample. (e) show a selected pixel for which we apply the Gaussian filter in (f). (g) shows the result of the Gaussian filter for the selected pixel.

Table B.2: Transition matrix

	Forest	Crop	Pasture
Forest	ff	fc	fp
Crop	cf	cc	cp
Pasture	pf	pc	pp

This matrix represents a generic transition matrix. The value (row,column) shows the conditional probability of the pixel transitioning from land use row to land use column.

pixel can only go back to being forest by going through the secondary vegetation land use. Once in the secondary vegetation, the pixel can go back to forest with a 1/30 probability of staying as secondary vegetation. This is a simple way to capture the fact that a secondary vegetation pixel return to most of it original carbon stock after 30 years.

Table B.3: Transition matrix with regeneration

	Forest	Crop	Pasture	Secondary Vegetation
Forest	ff	fc	fp	0
Crop	0	cc	cp	cf
Pasture	0	pc	pp	pf
Secondary Vegetation	(1/30)ff	fc	fp	(29/30)ff

This matrix represents a generic transition matrix for the scenario with regeneration. The value (row,column) shows the conditional probability of the pixel transitioning from land use row to land use column.

C Forest regeneration

In our model, an agent can cease farming operations in a field, which transitions the observed land cover back to forest. This gives rise to endogenous regeneration of the forest. We provide evidence that this flow of land from agriculture back to forest is sizeable. We also outline possible mechanisms, some not captured directly by our model, that provides further evidence that ceasing agricultural operations and letting the forest retake the field may reflect sound business decisions. We also complement data from the Mapbiomas project with two new modules: forest regeneration data and pasture quality data.

Regeneration and secondary vegetation. In the forest regeneration module, the Mapbiomas project (MapBiomas, 2019) identifies plots previously deforested but transitioning from an agricultural land use to secondary vegetation. Plots at the beginning of this transition, when vegetation is still not predominant, are classified in the *regeneration* state. When plots have completed the transition and are predominantly covered by natural vegetation, they are classified as *secondary vegetation*.

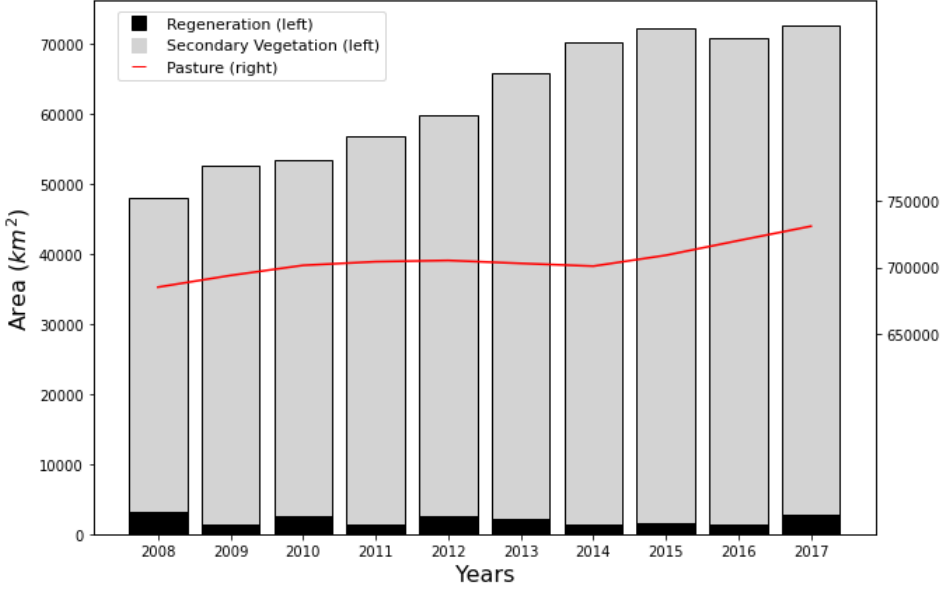
Figure C.1 shows the total area in our sample classified as either secondary vegetation or regeneration. Between 45,000 and 70,000 square kilometers in our sample are secondary vegetation. To compare the magnitude, Figure C.1 plots the total area dedicated to pasture grazing. We can conclude that secondary vegetation and regeneration are indeed important types of land use in the Brazilian Amazon in unprotected areas. In our model, both areas are bunched in the ‘forest’ land use.

This transition from agricultural activities back to vegetation is present in all regions of the Amazon where agricultural activities take place. Figure C.2 shows the location of secondary vegetation or regeneration.

Mechanisms. There is a range of possible mechanisms underlying this movement from agriculture to secondary vegetation. However, research on this topic is scant to the best of our knowledge. In our model, a farmer may decide to leave a plot fallow whenever agricultural activities become unprofitable. This could happen in practice due to a decline in soil health or reduced profitability. Farmers may deforest a plot of land and explore it as pasture grazing in an unsustainable way, degrading the soil over time. Once the soil is severely degraded, it can become uneconomical to keep a plot as a grazing area and the plot is abandoned, initiating the regeneration process discussed above.

We assess this mechanism using data on land degradation (MapBiomas, 2019). We regress a dummy variable of whether the pixel is classified as secondary vegetation or regeneration

Figure C.1: Regeneration and secondary vegetation



This figure depicts the total area classified as forest regeneration and secondary regeneration (left scale) in our sample over time. For comparison, we also plot total pasture area (right scale).

on dummy variables for each possible degradation status of pasture land in the previous year:

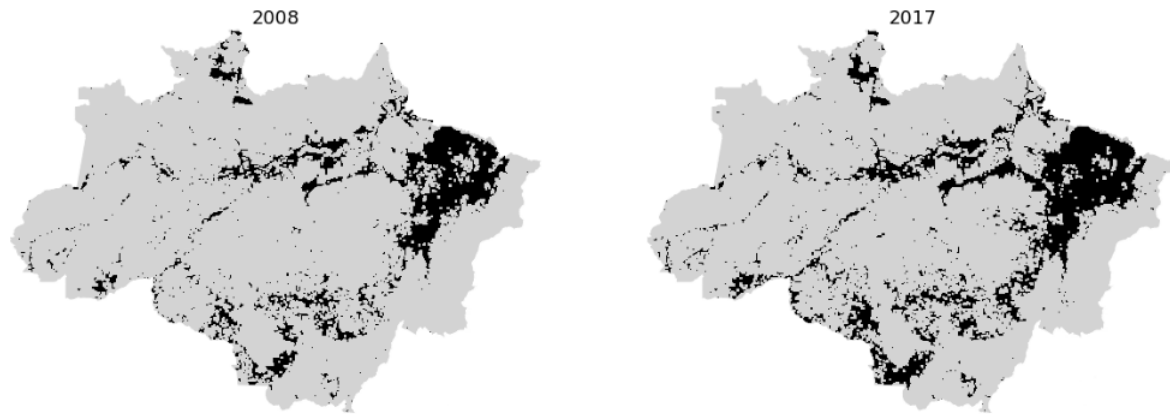
$$reg_{i,t+1} = \beta_0 no_deg_{i,t} + \beta_1 deg_{i,t} + \beta_2 severe_deg_{i,t} + \delta_t + X'_{i,t} \gamma + \epsilon_{i,t}, \quad (C.1)$$

where $reg_{i,t+1}$ is a dummy variable equal to 1 if pixel i in year $t+1$ is classified as secondary vegetation or regeneration; $no_deg_{i,t}$, $deg_{i,t}$, $severe_deg_{i,t}$ denote dummy variables for pixel i that is used as pasture grazing in year t classified with no pasture degradation, pasture degradation, and severe pasture degradation respectively; $X_{i,t}$ is a vector of controls (including soil suitability for soybeans and maize, pasture suitability index, and transportation cost); and δ_t represent year fixed effects.

Table C.1 presents the estimates from equation (C.1). We find that severely degraded pasture in t is more likely to transition to the forest state (that is, regeneration or secondary vegetation) in $t+1$ than pasture classified as just degraded, which in turn is more likely to transition to forest than non-degraded pasture. This suggests that forest regeneration is related to unsustainable use of the land and is, therefore, an economic choice. This is in line with evidence in Pendrill et al. (2022).

Besides pasture degradation, other mechanisms outside our model could explain the phenomenon of regeneration. For instance, land grabbers see deforestation as a portfolio management activity. Land grabbers may deforest multiple plots of land in hope that only

Figure C.2: Secondary vegetation map



This figure shows maps with the location of secondary vegetation. We reduce the resolution of the data to 15km to improve visualization.

some will be embargoed or caught by authorities. Those embargoed plots are abandoned, while the non-embargoed plots are sold and used for agriculture. Notice that the value of the land in illegal markets is closely linked to the profitability of that specific land. As land use in our model is a choice over the net present value of the flow of profits from the different land use, it captures in part deforestation for speculation purposes – i.e., land grabbers are more likely to speculate on more profitable land pondering the probability of being caught. Unfortunately, investigating this mechanism requires microdata from illegal activities which are not available.

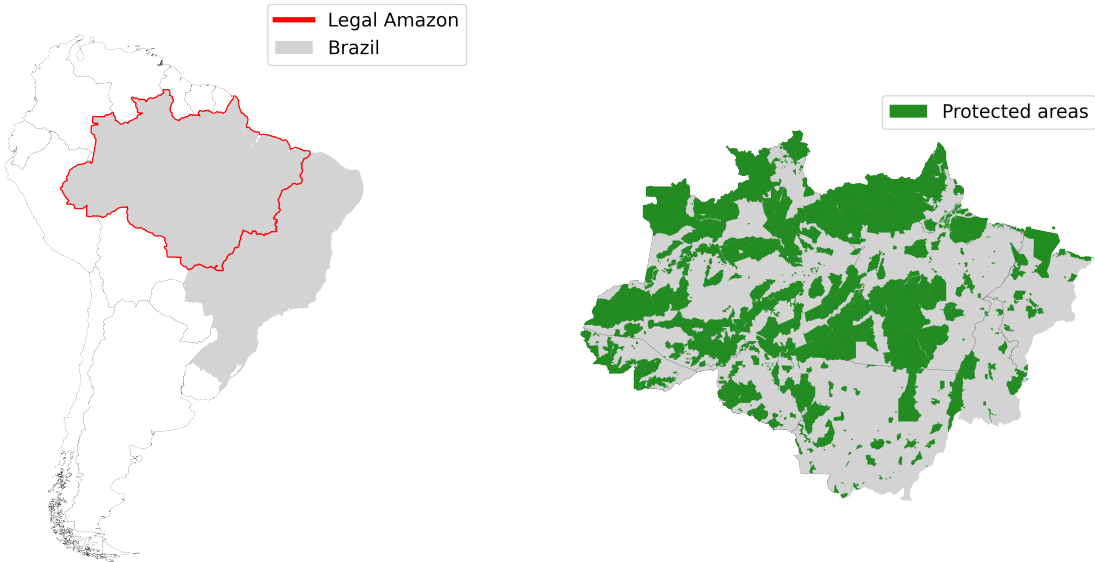
Table C.1: Regeneration and pasture degradation

	Estimate
No degradation	0.016 (0.0002)
Degradation	0.023 (0.0002)
Severe Degradation	0.045 (0.0002)
Soil Suitability	Yes
Transportation cost	Yes
Year FE	Yes

This table shows the results of regressing a dummy variable indicating whether the pixel in year $t + 1$ was classified as either secondary vegetation or regeneration on different pasture degradation statuses in year t (no degradation, degradation, or severe degradation of the pasture). The omitted category is when the pixel is not being used for pasture. Controls are soil suitability for soybeans and maize, pasture suitability index, and transportation cost. We also include year fixed effects. Standard errors in parentheses are clustered at the location level.

D Appendix Figures and Tables

Figure D.1: Legal Amazon Excluding Protected Areas (in green)



The figure shows Brazil, the Legal Amazon territory, and the protected areas (the green area in the map on the right). Our sample consists of the Legal Amazon area excluding the protected areas marked in green.

Table D.1: Soy and maize potential yield measured in Brazilian Reais for each year

Year	Maize suitability (R\$/ha)	Soy suitability (R\$/ha)
2008	2,396.91 (607.3)	2,564.78 (447.2)
2009	1,890.46 (478.99)	2,499.75 (435.86)
2010	1,826.58 (462.8)	2,009.81 (350.43)
2011	2,417.56 (612.54)	2,191.69 (382.15)
2012	2,245.75 (569.0)	2,944.67 (513.44)
2013	1,919.84 (486.43)	2,751.34 (479.73)
2014	1,796.17 (455.09)	2,556.35 (445.73)
2015	1,754.67 (444.58)	2,440.59 (425.55)
2016	2,527.68 (640.44)	2,601.58 (453.62)
2017	1,681.91 (426.15)	2,160.53 (376.71)

This table shows the average and mean of soy and maize potential yields ($y_{m,maize}, y_{m,soy}$) multiplied by their prices ($p_{maize,t}, p_{soy,t}$) for each year from 2008 to 2017.

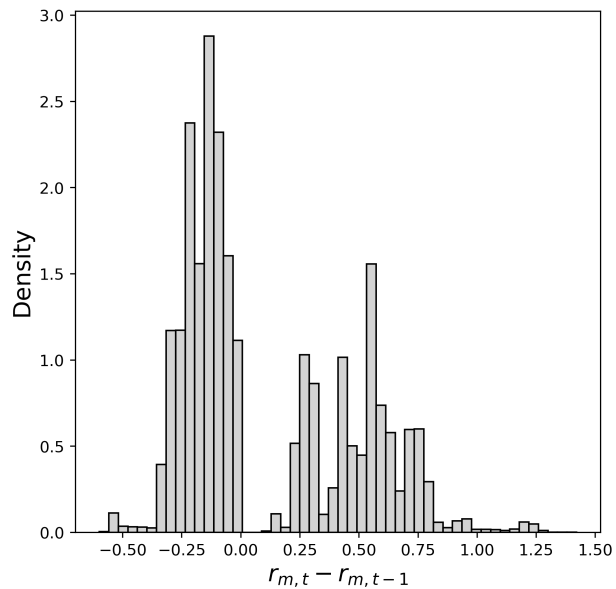


Figure D.2: This figure plots the histogram of the return in difference of the variable $(r_{m,t} - r_{m,t-1})$, showing substantial cross-sectional variation. Notice that the distribution is bimodal, since the sign of the variable depends on whether the prices of maize and soybeans increased or decreased between years. The mean value is 0.11 with a standard deviation of 0.36

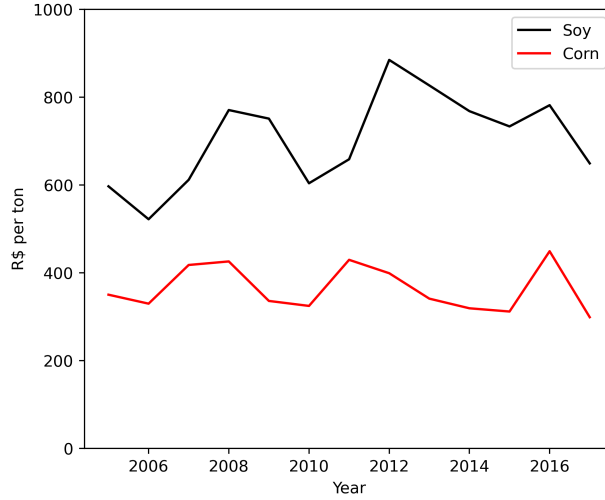


Figure D.3: This figure shows the evolution of prices for soybeans and maize over our study period. We estimated AR(1) processes for these two series as a first check of stationarity. Estimated AR(1) auto-regressive coefficients are -0.18 (0.24, S.E.) and 0.25 (0.25, S.E.) respectively for maize and soy. Therefore, both processes display relatively low auto-regressive coefficients, which are consistent with stationary processes. The Augmented Dickey-Fuller test rejects non-stationarity in favor of stationarity for maize (p-value: 0.01) and soy (p-value: 0.07) at 10% significance level. Although the test provides weaker evidence for soy price stationarity, we highlight we use a very short time series in our setting. Moreover, the model's time-dependent state variable is r_{mt} , which is a weighted average of maize and soy returns. Therefore, the persistence of r_{mt} should be between that of maize and soy, which provides greater confidence that actual time-varying model state variables are stationary as required by the analysis.

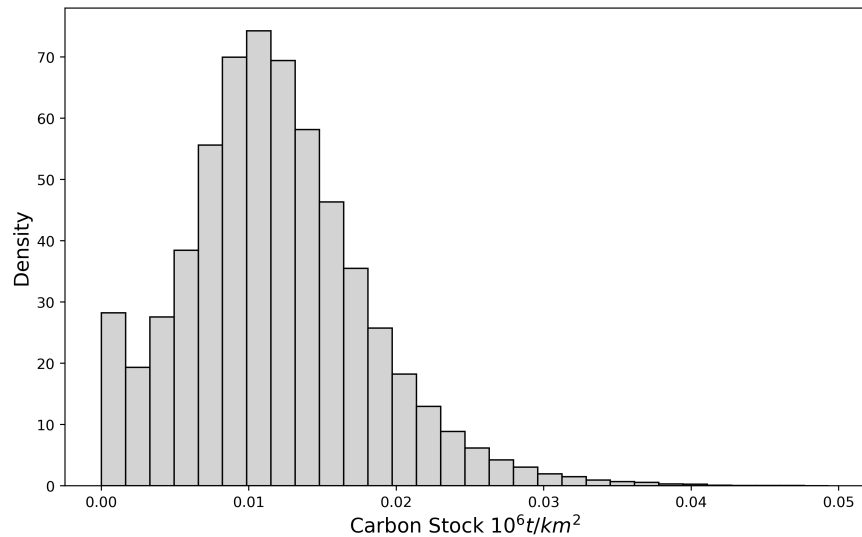


Figure D.4: This figure shows the distribution of the carbon stock data described in Table 2 and Figure 1.

Table D.2: Within estimation: First stage

Regressor	(1)	(2)	(3)	(4)	(5)	(6)
$\tilde{r}_{i,t-2}$	0.041 (0.001)	0.046 (0.001)	0.041 (0.001)	0.041 (0.001)	0.041 (0.001)	0.041 (0.001)
$W_{j,k,i,2011}$	-0.033 (0.001)	-0.048 (0.001)	-0.033 (0.001)	-0.031 (0.001)	-0.033 (0.001)	-0.033 (0.001)
$W_{j,k,i,2012}$	-0.001 (0.001)	-0.035 (0.001)	-0.001 (0.001)	-0.009 (0.001)	-0.003 (0.001)	-0.001 (0.001)
$W_{j,k,i,2013}$	0.029 (0.001)	0.054 (0.001)	0.029 (0.001)	0.030 (0.001)	0.029 (0.001)	0.029 (0.001)
$W_{j,k,i,2014}$	0.017 (0.001)	0.040 (0.001)	0.017 (0.001)	0.020 (0.001)	0.018 (0.001)	0.017 (0.001)
$W_{j,k,i,2015}$	0.010 (0.001)	0.026 (0.001)	0.010 (0.001)	0.012 (0.001)	0.011 (0.001)	0.010 (0.001)
$W_{j,k,i,2016}$	-0.043 (0.001)	-0.061 (0.001)	-0.043 (0.001)	-0.040 (0.001)	-0.043 (0.001)	-0.043 (0.001)

This table presents the first stage estimates using the lagged values $\tilde{r}_{i,t-2}$ as an instrument for $X_{j,k,i,t}$. The first column reports regressors. Standard errors in parenthesis were computed with block bootstrap with 1000 iterations in a grid of 25km by 25km. Number of observations for Estimate (1),(2),(3),(6) is 79,478,568. Number of observations for Estimate (4) is 8,457,480. Number of observations for Estimate (5) is 6,7151,376. Estimate (1) shows the results when the crop revenue net of transportation cost is a weighted average of soy and maize, where the weights are the proportion of the product in the region that the pixels lies inside. Estimate (2) shows the result when we consider that every pixel will apply a double crop system, producing soy and maize of second season in the same year. Estimate (3) shows the result for the scenario where the discount rate is $\rho = 0.95$, instead of $\rho = 0.9$. Estimate (4) shows the result for the scenario where we only use as sample the pixels that were already deforested in 2008. Estimate (5) shows the result when we exclude the pixel within peatlands. Estimate (6) shows the result for the static version of the model.

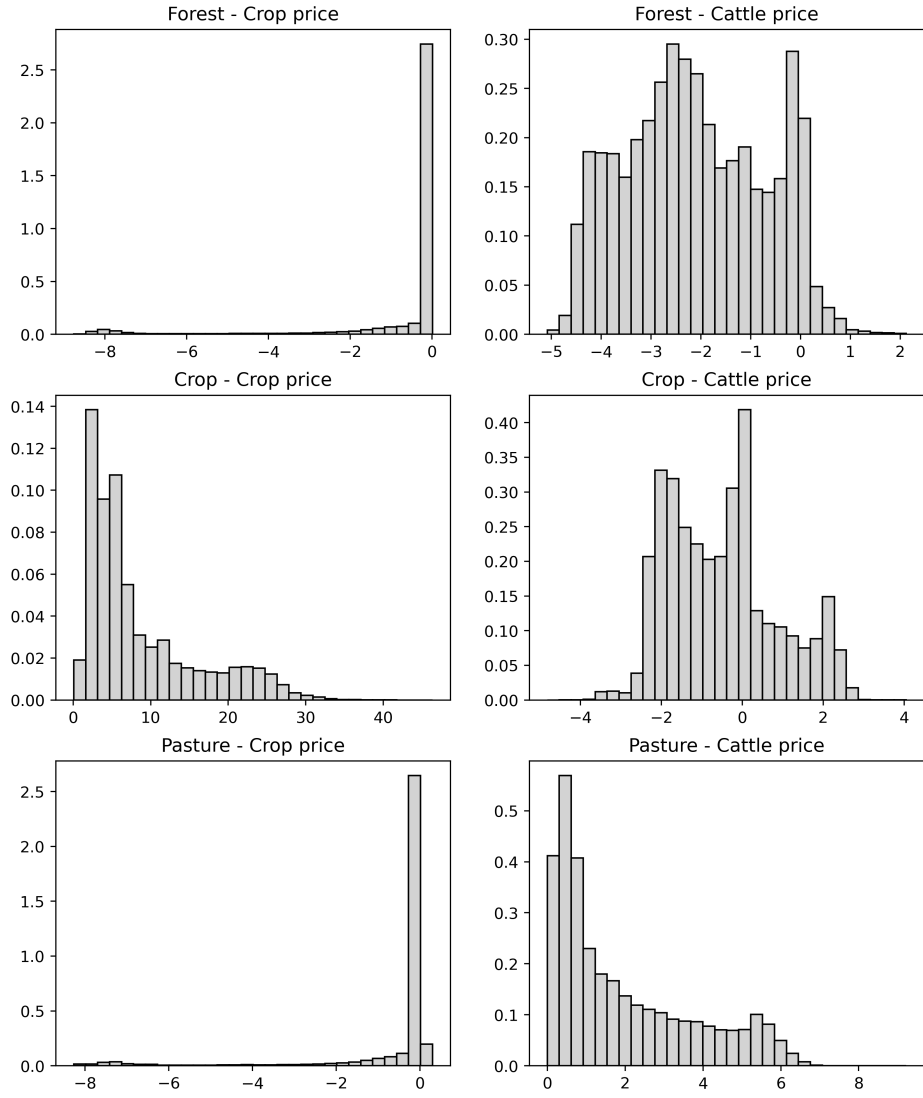


Figure D.5: These plots show the elasticity of each land use (forest, crop, and pasture) to different changes in prices (crop and cattle price). The x-axis of each plot is the elasticity of the land use with respect to crop or pasture price. This is a disaggregated result of Table 5, as such we use a 10% increase in prices to compute the elasticities. Notice that in this disaggregated form we do not need to show the elasticity of carbon with respect to crop or pasture prices, since in this disaggregated form this elasticity is numerically equal to the forest one.

Table D.3: Effects of different levels of carbon tax for forestation and carbon emissions

Carbon tax (\$/ton)	Δ Forest cover ($1,000km^2$)	ΔCO_2 released (gigatons)
(1)	(2)	(3)
\$2.5	526 (21.3)	-25 (0.9)
\$ 5	766 (23.0)	-34 (1.1)
\$ 10	966 (24.2)	-40 (1.3)
\$ 20	1100 (25.9)	-42 (1.5)

This table presents counterfactual results for the increase in forested area and decrease in emissions for different values of carbon taxes imposed on agents. Our baseline perceived carbon value implied by the model estimates is 2.74 \$/t CO_2 . Here, we consider smaller carbon tax values – 2.5, 5, 10, and 20 \$/t CO_2 – added to the perceived baseline carbon value. The column Δ Forest cover gives the difference of steady-state forest cover between the baseline scenario and the alternative scenario. The ΔCO_2 released column gives the total difference of CO_2 released between the baseline and the alternative steady state scenario for all pixels we consider in our sample. Standard errors in parenthesis were computed with block bootstrap with 1000 iterations in a grid of 25km by 25km.

Table D.4: Extensions – Crop flow profit coefficient

Regressor	Model Parameter	(1)	(2)	(3)	(4)	(5)	(6)
$X_{j,k,i,t}$	α_{crop}	0.392 (0.016)	0.217 (0.008)	0.367 (0.016)	0.174 (0.017)	0.381 (0.014)	0.838 (0.017)
$W_{j,k,i,2011}$	$\Delta\alpha_{pasture,2011}^1$	0.034 (0.001)	0.033 (0.001)	0.035 (0.001)	0.048 (0.001)	0.038 (0.001)	0.032 (0.001)
$W_{j,k,i,2012}$	$\Delta\alpha_{pasture,2012}^1$	-0.011 (0.001)	-0.003 (0.001)	-0.010 (0.001)	-0.006 (0.001)	-0.011 (0.001)	-0.021 (0.001)
$W_{j,k,i,2013}$	$\Delta\alpha_{pasture,2013}^1$	-0.039 (0.002)	-0.039 (0.001)	-0.039 (0.002)	-0.055 (0.002)	-0.042 (0.001)	-0.036 (0.001)
$W_{j,k,i,2014}$	$\Delta\alpha_{pasture,2014}^1$	0.030 (0.002)	0.029 (0.002)	0.031 (0.002)	0.016 (0.002)	0.027 (0.002)	0.008 (0.001)
$W_{j,k,i,2015}$	$\Delta\alpha_{pasture,2015}^1$	-0.055 (0.001)	-0.055 (0.001)	-0.056 (0.001)	-0.018 (0.001)	-0.047 (0.001)	-0.038 (0.001)
$W_{j,k,i,2016}$	$\Delta\alpha_{pasture,2016}^1$	0.058 (0.001)	0.055 (0.001)	0.057 (0.001)	0.025 (0.001)	0.052 (0.001)	0.074 (0.001)

This table shows the estimates of α_{crop} obtained in the second stage regression (equation 16) using Anderson and Hsiao (1981) estimator. Estimate (1) shows the result of our baseline specification. Estimate (2) shows the result when we consider that every pixel will apply a double crop system, producing soy and maize of second season in the same year. Estimate (3) shows the result when the discount factor is set to $\rho = 0.95$ instead of $\rho = 0.9$. Estimate (4) shows the result for the scenario where we only use as sample the pixels that were already deforested in 2008. Estimate (5) shows the result when we exclude the pixel within peatlands. Estimate (6) shows the result for the static version of the model. The first column reports regressors, while the second column displays the corresponding model parameters from Section 3.2, equations (14) and (15). Standard errors in parenthesis were computed with block bootstrap with 1000 iterations in a grid of 25km by 25km. Number of observations for Estimate (1),(2),(3),(6) is 79,478,568. Number of observations for Estimate (4) is 8,457,480. Number of observations for Estimate (5) is 67,151,376.

Table D.5: Extensions – Forest and pasture flow profits coefficients

Regressor	Model parameter	(1)	(2)	(3)	(4)	(5)	(6)
h_m	α_{forest}	4.41 (0.32)	6.21 (0.27)	4.14 (0.32)	2.48 (0.22)	4.53 (0.29)	9.29 (0.61)
$h_m \mathbf{1}\{k = forest\}$	$(1 - \rho)\varphi$	-4.18 (0.09)	-4.18 (0.09)	-1.27 (0.05)	-1.88 (0.06)	-3.87 (0.09)	-56.56 (0.97)
$W_{j,k,m}$	$\alpha_{pasture, 2011}^1$	0.06 (0.01)	0.08 (0.01)	0.06 (0.01)	0.09 (0.01)	0.06 (0.01)	0.19 (0.01)
$W_{j,k,m} d_m$	$\alpha_{pasture}^2$	-0.00 (0.01)	-0.00 (0.01)	-0.00 (0.01)	-0.00 (0.01)	-0.00 (0.01)	0.00 (0.01)
Intercepts							
	$(1 - \rho)\Phi(past, forest)$	-0.46 (0.01)	-0.46 (0.01)	-0.26 (0.01)	-0.55 (0.01)	-0.47 (0.01)	-4.13 (0.04)
	$(1 - \rho)\Phi(crop, forest)$	-0.81 (0.01)	-0.81 (0.01)	-0.38 (0.01)	-0.82 (0.01)	-0.80 (0.01)	-8.49 (0.03)
	$(1 - \rho)\Phi(crop, past)$	-0.60 (0.01)	-0.60 (0.01)	-0.28 (0.01)	-0.51 (0.01)	-0.58 (0.01)	-6.26 (0.03)
	$(1 - \rho)\Phi(past, crop)$	-0.20 (0.01)	-0.20 (0.01)	-0.12 (0.01)	-0.25 (0.01)	-0.21 (0.01)	-1.65 (0.02)
	$\bar{\alpha}_{pasture}$	0.13 (0.01)	0.11 (0.01)	0.04 (0.01)	0.13 (0.01)	0.14 (0.01)	1.72 (0.02)
	$\bar{\alpha}_{crop}$	-0.66 (0.04)	-0.70 (0.04)	-0.78 (0.04)	-0.18 (0.04)	-0.62 (0.04)	1.52 (0.06)

This table presents the OLS estimates of equation (10), using $\hat{\alpha}_{crop}$ and $\Delta\alpha_{pasture,t}^1$ estimated in equation (16) using Anderson and Hsiao (1981). Estimate (1) shows the result of our baseline specification. Estimate (2) shows the result when we consider that every pixel will apply a double crop system, producing soy and maize of second season in the same year. Estimate (3) shows the result when the discount factor is set to $\rho = 0.95$ instead of $\rho = 0.9$. Estimate (4) shows the result for the scenario where we only use as sample the pixels that were already deforested in 2008. Estimate (5) shows the result when we exclude the pixel within peatlands. Estimate (6) shows the result for the static version of the model. The first column reports regressors, while the second column displays the corresponding model parameters from Section 3.2, equations (14) and (15). Standard errors in parenthesis were computed with block bootstrap with 1000 iterations in a grid of 25km by 25km. Number of observations for Estimate (1),(2),(3),(6) is 79,478,568. Number of observations for Estimate (4) is 8,457,480. Number of observations for Estimate (5) is 67,151,376.

Table D.6: Extensions – Efficient forestation and counterfactual carbon tax

Carbon tax	Δ Forest cover (1,000km ²)	ΔCO_2 released (billion tons)
(1)	(2)	(3)
Panel A. Double cropping agriculture		
\$ 2.5	291	-14
\$ 5.0	488	-23
\$ 10.0	709	-30
\$ 20.0	891	-35
\$43.0	1026	-37
Panel B. Discount rate ($\rho = 0.95$)		
\$ 2.5	639	-32
\$ 5.0	934	-43
\$ 10.0	1163	-49
\$ 20.0	1309	-52
\$ 47.3	1394	-53
Panel C. Subsample		
\$ 2.5	233	-12
\$ 5.0	487	-24
\$ 10.0	891	-43
\$ 20.0	1215	-54
\$ 46.5	1408	-58
Panel D. Peatland		
\$ 2.5	573	-28
\$ 5.0	851	-39
\$ 10.0	1077	-46
\$ 20.0	1227	-49
\$ 47.1	1323	-50
Panel E. Static		
\$ 2.5	228	-9
\$ 5.0	331	-13
\$ 10.0	451	-17
\$ 20.0	562	-19
\$ 47.3	660	-20

This table presents counterfactual results for the increase in forested area and decrease in emissions for different values of carbon taxes imposed on agents for five model extensions. Panel A shows the result when we consider that every pixel will apply a double crop system, producing soy and maize of second season in the same year. Panel B shows the results derived using a discount factor of $\rho = 0.95$ instead of $\rho = 0.9$. Panel C shows the results derived when we only use as sample the pixels that were already deforested in 2008. Panel D shows results derived when we exclude pixels inside peatlands. Panel E shows results for the static model. The column Δ Forest cover gives the difference of steady-state forest cover between the baseline scenario and the alternative scenario. The ΔCO_2 released column gives total the difference of CO_2 steady-state released between the baseline and the alternative scenario for all pixels we consider in our sample.

Table D.7: Extensions – Carbon accounting with forest regeneration

Carbon tax (US\$/ton)	Share of forest < 30 yrs	ΔCO_2 released (billlion tons)
(1)	(2)	(3)
\$ 0.0†	0.48	0.00
\$ 2.5	0.33	-25.92
\$ 5.0	0.25	-39.11
\$ 10.0	0.17	-49.23
\$ 20.0	0.12	-55.19
\$ 47.3‡	0.06	-58.66

This table presents results for avoided emissions from different carbon taxes for an alternative scenario in which secondary vegetation (forest recently converted from pasture and crops) stays 30 years with zero carbon stock, realizing its full potential after 30 years. Column (2) presents out of the total forest area in the long run, the share which is secondary vegetation (age < 30 years). First row (†) displays the status quo scenario and the last row (‡) the efficient forestation scenario.

Table D.8: Land Use and Emissions for First and Second Best Policies

Scenario	Forest	Crop	Pasture	Emissions
BAU	958	103	1,144	42
First Best - BAU	1,186	-97	-1,088	-42
Second Best - BAU	971	35	-1,007	-38

This table shows land use for forest, crop, and pasture and total emissions. The first row shows results for the business-as-usual scenario. Second and third rows show results relative to the business-as-usual scenarios considering first and second best policies. Units are in thousand km^2 for land use and billion CO_2 for emissions.